Journal of Hydrology 638 (2024) 131490

Contents lists available at ScienceDirect

Journal of Hydrology

journal homepage: www.elsevier.com/locate/jhydrol

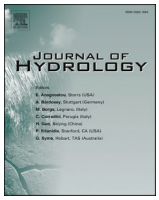

Research papers

A new approach to net solar radiation in a spatially distributed snow energy balance model to improve snowmelt timing

Joachim Meyer [a,*], Andrew Hedrick [b], S. McKenzie Skiles [a]

[a] Department of Geography, University of Utah, Salt Lake City, UT, USA
[b] Northwest Watershed Research Center, USDA Agricultural Research Service, Boise, ID, USA

A B S T R A C T

Snow that accumulates seasonally in mountain headwaters is traditionally a vast and consistent natural reservoir, providing water as the snow melts in the spring and summer. This resource is at risk due to declining and more variable snow cover, increasing the need to accurately forecast snowmelt. The timing and magnitude of snowmelt, first order controls on downstream water resources, are primarily driven by the amount of absorbed (net) solar radiation controlled by the snow albedo. However, solar radiation and snow albedo are not commonly measured at mountain instrumentation sites despite their high degree of spatial variability. With the sparsity of observations, physically based snow models often use simplified solar radiation modeling and time-decay albedo functions, leading to errors in snowmelt rate and snow depletion timing. Here, this limitation has been addressed by combining two independent gridded solar radiation data products; 1) incoming solar radiation output from the High-Resolution Rapid Refresh (HRRR; U.S. National Weather Service) numerical weather prediction model and 2) remotely sensed snow albedo derived from the Moderate-Resolution Imaging Spectroradiometer (MODIS). The hourly HRRR and snow albedo products were used to update net solar radiation in a spatially distributed snow energy balance model over two water years (2021, 2022) in the East River Watershed, Colorado, USA. Results were assessed through time against two observation sites within watershed boundaries and spatially against snow extent from two airborne lidar flights in 2022. Updating net solar radiation improved modeling of melt rates and reduced errors in snow depletion timing from 15 – 33 days later (baseline runs) to 1 – 6 days later relative to the observation sites. The updates additionally improved spatial agreement of where snow had already been depleted from 87% to 97% during the melt season relative to lidar. These enhancements using open-access gridded products available over the continental US increase the potential for adaptation of process-based models into local water supply forecast operations to ultimately improve runoff predictions in snow dominated watersheds.

1. Introduction

Observation studies have established that net solar radiation, controlled by snow albedo, acts as a large source of energy for melt in most snow environments (Marks and Dozier, 1992, DeWalle and Rango, 2008). Relatedly, from global to local point-scale models, correctly representing change in snow albedo over time has been shown to be critical for accurately modeling snow energy balance, melt rates, and extent during ablation. The traditional approach of representing albedo, an empirical 'time since snowfall' nonlinear decay function, leads to errors in climate models (Qu and Hall, 2014), land surface models (Chen et al., 2014; Ryken et al., 2020), hydrological models (Clark et al., 2015), and snow models (Krinner et al., 2018; Schmucki et al., 2014). Alternative snow albedo model representations, such as snow surface temperature-based decay or with varying decay rates during snow melt have been implemented, but still lack the ability to accurately represent snow albedo over time (Pedersen and Winther, 2005). More complex snow albedo simulations in radiative transfer models also consider controlling factors such as cloud optical thickness or solar zenith angle (Gardner and Sharp, 2010), but have yet to be included with large-scale spatially distributed models. The basis of the time-based representation is that snow albedo is highest for freshly fallen snow, and then declines over time as snow grain size increases due to metamorphic processes. Grain size, though, only determines snow albedo in near infrared wavelengths where ice is absorptive (Wiscombe and Warren, 1980). In visible wavelengths, where ice is transparent and snow is highly scattering, albedo is related to surface darkening by light absorbing particles (LAP).

The variability in grain growth rates and accumulation of LAPs consequently introduces variability in snow albedo and rates of decline that cannot be uniformly represented by a time-based approach. For example, grain growth is not consistent, exhibiting faster growth in the presence of liquid water (Donahue et al., 2021), warmer air temperatures (Kaempfer and Schneebeli, 2007), and darkening by LAPs (Skiles and Painter, 2017) – all properties of which vary within a watershed over space and time. The timing and impact of LAPs is not easily predicted, varying for example with emissions of dust from arid and disturbed landscapes, black carbon from anthropogenic sources and

* Corresponding author.
E-mail address: j.meyer@utah.edu (J. Meyer).

https://doi.org/10.1016/j.jhydrol.2024.131490
Received 22 September 2023; Received in revised form 22 May 2024; Accepted 27 May 2024
Available online 13 June 2024

wildfire, and algae growth. Even when an area is known to consistently receive dust on snow deposition, like the Colorado Rocky Mountains in Colorado, USA, there is high interannual variability in the timing and amount deposited (Skiles et al., 2012). Furthermore, the albedo of freshly fallen snow itself exhibits spatial and temporal variability (Skiles et al., 2023) and does not reset to the same value (Abolafia-Rosenzweig et al., 2022). The time-based decay functions continue to be applied, though, because snow albedo and controlling processes are notoriously challenging to observe and parameterize in models (Bair et al., 2019).

Incorrect albedo values propagate directly to the model results by modulating the absorbed solar radiation. If snow albedo is too high, for example, absorbed solar radiation will be too low and the snow will melt too slowly (Chen et al., 2014). This has direct implications for modeling snowmelt timing and forecasting water availability. Absorbed, or net solar radiation (R_S), in physically based snow models is calculated via the following equation:

$$R_S = (1 - \alpha) \times S_i \quad (1)$$

Where α is the snow albedo, the unitless ratio that indicates the fraction of reflected to incoming solar radiation, such that the term (1- α) is the co-albedo, or the fraction of incoming sunlight that is absorbed by the snowpack. When multiplied by S_i, the incoming solar radiation (Wm^{-2}), the result is the total or net amount of solar radiation absorbed by the snowpack (Wm^{-2}). Net solar radiation is a term in the overall snowpack energy balance (Q) :

$$Q = NS + NL + H + L + G + M \quad (2)$$

Where NS is net solar, NL is net longwave, H is sensible heat, L is latent heat, G is conductive heat (soil-snow interface), and M is the advected heat (precipitation) energy transfer term (all terms are in Wm^{-2}) (Marks and Dozier, 1992). A common approach to solve for net solar in process-based models is to calculate incoming solar radiation with a topographically adjusted theoretical model (i.e., two-stream model, Dozier and Frew, 1990), adjusted with a cloud factor, and the time-decay function for snow albedo. To improve the representation of net solar the options are to improve the representation of incoming solar radiation, snow albedo, or both.

In the current literature, different approaches have improved snowmelt timing from snow models through advanced snow albedo representation. Skiles and Painter (2019) added in situ measured dust information to individual layers simulated with the physical based SNOWPACK model (Bartelt and Lehning, 2002). The dust data were subsequently included in a radiative transfer model to derive snow albedo, replacing the default time-decay method of the model. This combination allowed snow depletion simulations within two days of the observation at a measurement station. Tuzet et al. (2017) extended a physical based snow model to use snow albedo from a radiative transfer model that used LAP information from an atmospheric model, which also brought the modeled snow melt-out dates closer to the observed. Niwano et al. (2021) forced the Snow Metamorphism and Albedo Process (SMAP; Niwano et al., 2014) model with LAP information from a meteorology-chemistry model. SMAP uses the physically based snow albedo model (PBSAM; Aoki et al., 2011) and also improved the accelerated snow melt simulation by including the LAP data. Oaida et al. (2015) used a radiative transfer model to inform the Simplified Simple Biosphere (SSiB-3) land surface model (LSM) coupled with the Weather Research and Forecasting/Advanced Research WRF (WRF-ARW), which used a built-in radiative transfer model to calculate albedo based on aerosol and grain growth rates, at 15 km spatial resolution. The modified SSiB-3 LSM setup is one of the few efforts to address the need to account for controls on snow albedo on larger spatial scales. They improved the difference between the observed and simulated snow disappearance from about one month to 13 days.

Malik et al. (2012) used a notably different approach, where the time-decay snow albedo values in the Noah land-surface model (Ek et al., 2003) were updated with observed data. The observations were from a Moderate Resolution Imaging Spectroradiometer (MODIS) product and updated the values while preserving the time-based albedo decay. The direct insertion updates mainly improved the simulated albedo after a long cycle without freshly fallen snow and had limited improvements to the snowmelt timing. While all the presented model modifications improved representation of snow processes, none of the assessments were designed or executed at the watershed scale with high (sub-kilometer) spatial resolution. This leaves an unaddressed need to investigate options for snow models aimed at hydrologic forecasting.

Given the spatial and temporal variability in snow albedo, remote sensing is the ideal candidate to provide relevant and timely data. Two widely used snow-specific remote sensing products are the outputs from the MODIS Snow-Covered Area and Grain size (MODSCAG; Painter et al., 2009) and MODIS Dust Radiative Forcing in Snow (MODDRFS; Painter et al., 2012) retrieval workflows. MODSCAG retrieves the fractional snow cover, snow grain size, and clean snow albedo per 500-meter pixel. MODDRFS determines visible albedo reduction, or snow darkening, due to the presence of LAP at the snow surface and resultant radiative forcing. The two albedo products can be combined, with clean snow albedo reduced by the snow darkening, to estimate the observed snow albedo. Both products have been widely used to validate snow property information of modeled results (Sarangi et al., 2019; Minder et al., 2016; Hao et al., 2022; Huang et al., 2022). So far, successful use of MODIS-based snow information as a model input has only been shown by Miller et al. (2016), who used radiative forcing to perturb net solar radiation within the 1-dimensional Snobal model, concluding with a call for methods that scale across large areas and extended time periods for hydrological forecasting.

Here, we present a workflow that directly inserts the MODIS observed snow albedo information into the spatially distributed iSnobal model (Marks et al., 1999), a pathway to fill the gap identified by Miller et al., 2016. Various studies have applied the iSnobal energy balance model across a range of spatial resolutions (Kormos et al., 2014; Marks et al., 1999; Garen & Marks, 2005) and in various snow environments spanning maritime (Hedrick et al., 2018, 2020), arctic (Winstral et al., 2009), intermountain (Marks and Winstral, 2001; Kiewiet et al., 2022; Hale et al., 2023), and continental snowpacks (Meyer et al., 2022, Bonnell et al., 2023). Additionally, we test improvements from using incoming solar radiation from the High-Resolution-Rapid-Refresh (HRRR; Dowell et al., 2022) numerical weather prediction (NWP) model. Meyer et al. (2023) showed well-simulated snow depth and mass balance during accumulation at the watershed scale when forced with meteorological outputs from HRRR. As with other snow models, the HRRR-iSnobal combination showed deficiency during the melt season, depleting the snow too slowly and too late, indicating a need to improve the modeled net solar radiation. This is addressed with the architecture presented here and demonstrated over a watershed (1373 km^2) in the headwaters of the Colorado River Basin. Three different HRRR-iSnobal combinations were assessed against in situ point measurements and spatial observations. This solution to updating snow albedo and net solar radiation is both scalable and accessible given the open-source model and open-access spatially gridded inputs.

2. Study area and years

The East River Watershed (ERW) is a high alpine environment located in the Upper Gunnison Watershed within the upper Colorado River Basin (CRB) (Fig. 1). The East River is one of the two primary tributaries of the Gunnison River, which itself discharges into the Colorado River. The ERW has an average elevation of 3266 m and vertical elevation relief of 1420 m (Hubbard et al., 2018) and a mixture of different vegetation types such as brush and grassland or mixed conifer and aspen trees. These characteristics are typically found in the mountain headwater watersheds of the CRB, which led to the designation of the ERW as a Scientific Focus Area (https://watershed.lbl.gov/) in 2016

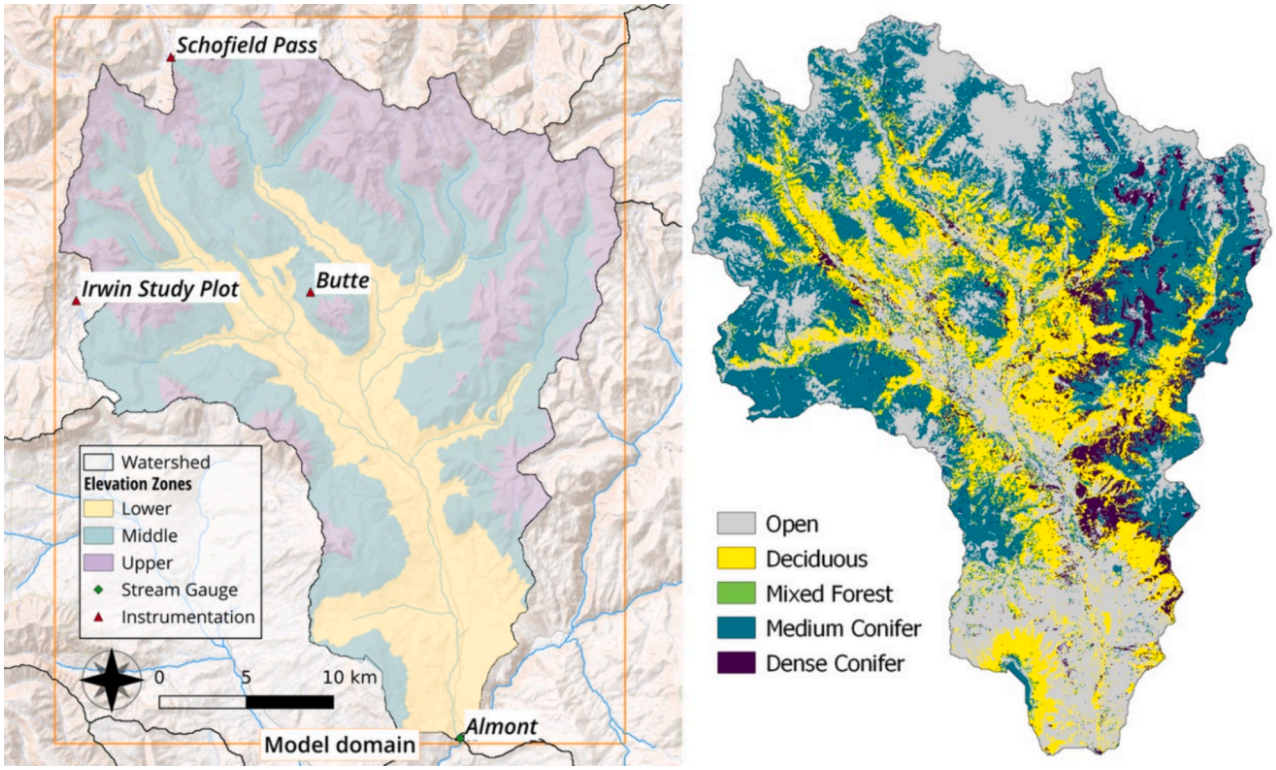

Fig. 1. Areal map of the East River Watershed (black outline) showing the model domain, elevation zones, and locations of the instrumentation sites (left). Map on the right shows the vegetation types within the model domain based on the LANDFIRE National Vegetation Classification, which are used as metadata in iSnobal radiation calculations.

and is supported by the US-DOE Biological and Environmental Research Subsurface Biogeochemistry Program.

The study period spanned water years 2021 and 2022 (Oct 1st – Sep 30th), and model inputs and outputs were assessed against in situ observations from three instrumentation sites located inside the ERW study domain. Two sites are part of the Snow Telemetry (SNOTEL) network operated by the United States Department of Agriculture National Resource Conservation Service (USDA-NRCS): Schofield Pass (elevation: 3261 m) and Butte (elevation: 3097 m). Based on the long-term SNOTEL record (30 years) for the sites, water year 2021 had below-average snow water equivalent (SWE) and earlier than typical snow melt timing. Water year 2022 also had earlier than typical snowmelt timing, despite a slightly above average SWE year, due to dust deposition and radiative forcing. The third instrumentation site was the Irwin Study Plot (3177 m), which recently was equipped with incoming and outgoing solar radiation observations by the University of Utah Snow Hydrology Research to Operations Laboratory. The ERW had additional aerial snow depth measurements by Airborne Snow Observatories Inc. (https://www.airbornesnowobservatories.com/) in 2022, which were used to assess how well snow patterns were modeled spatially.

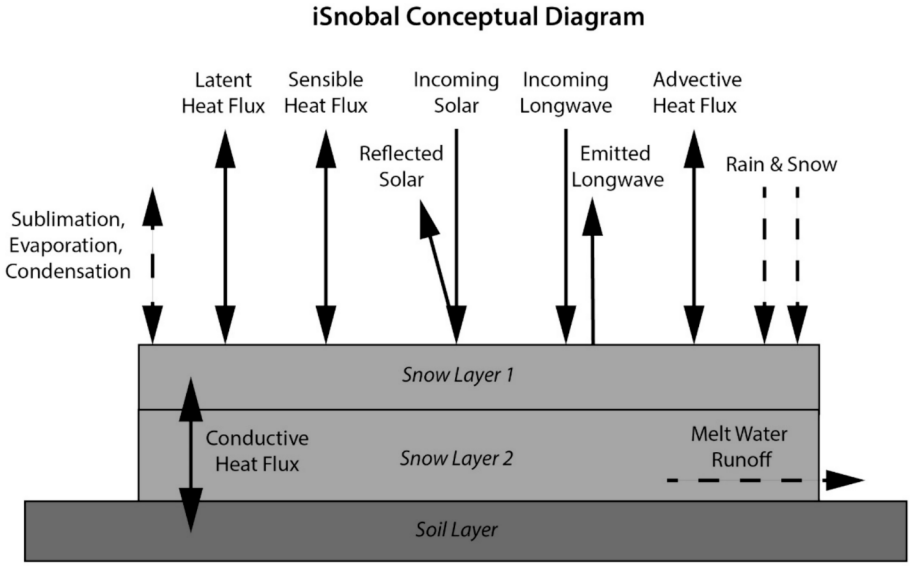

Fig. 2. Diagram of the iSnobal model snowpack architecture and simulated mass (dashed arrows) and energy (solid arrows) fluxes.

3. Model and data

3.1. Model setup

The iSnobal model simulates snowpack evolution by resolving energy and mass balance fluxes. The two-layer model calculates the snowpack net radiative, sensible, latent, conductive, and advective energy fluxes for a preconfigured time step (Fig. 2). Once the net energy fluxes deplete the cold content (the energy required to raise the temperature to 0 °C) and the snow meltwater amount exceeds the maximum liquid water holding capacity of the snowpack, the meltwater outflow is calculated. The model stores the simulated state variables of the snowpack (i.e., snow depth, snow density, meltwater, etc.) as summary statistics after a regular (and configurable) time interval has passed. These state variables then serve as initialization values once a simulation continues and new energy fluxes change the snowpack.

A complete setup of the model requires the overarching Automated Water Supply Model (AWSM; Havens et al., 2020) software that combines the Spatial Modeling for Resource Framework (SMRF; Havens et al., 2017) and iSnobal into one framework (Fig. 3a). The external Katana module is a wrapper for the WindNinja downscaling approach (Forthofer et al., 2014), which assists in refining the supplied HRRR wind data (3 km spatial resolution) to a higher resolution (200 m) accounting for the modeled topography. The model installation, model domain preparation, and daily model execution is described in more detail in Meyer et al. (2023).

For this work, the HRRR-iSnobal combination was set to simulate hourly updates at 50 m spatial resolution, storing the state variables at the end of each day. The chosen spatial resolution resulted in a modeled domain of 837 x 656 grid cells to cover the ERW area of 1373 km^2. This model configuration was identical to Meyer et al. (2023).

3.2. Forcing data

To simulate the snowpack mass and energy fluxes, iSnobal requires the meteorological inputs of: air temperature, relative humidity, incoming solar radiation, wind speed and direction, and total precipitation. These variables, along with additional required forcing information (e.g. longwave radiation, precipitation phase, etc), are prepared for the model domain by SMRF. The meteorological values are available from the HRRR NWP model, which produces hourly forecasts up to 18-hours at 3 km spatial resolution. The HRRR model became a U. S. National Weather Service's (NWS) operational forecast model in late 2014 and covers the continental United States and Alaska. There have been four versions of HRRR since becoming one of the production models for the NWS and distribution of the last and final HRRRv4 version started in late 2021. HRRRv4 brought advances to cloud physics and modeled solar radiation at the surface (James et al., 2022), which guided the selection of the simulated water years for this study (2021 and 2022). Additionally, using meteorological inputs from one HRRR product version reduced the potential of possible error sources comparing the different iSnobal input forcing combinations.

3.3. HRRR solar radiation product

Using the HRRR forecast products as forcing inputs for iSnobal provided the additional opportunity to evaluate the HRRR Downward Short-Wave Radiation Flux (DSWRF) variable as an alternative source to the current SMRF implementation (Section 3.5.1.2). The DSWRF variable in HRRRv4 saw a bias reduction of up to 50 % compared to HRRRv3, which was evaluated against local instrumentation sites in the lower 48 United States (James et al., 2022). An additional extensive HRRRv4 near surface outputs evaluation, that included the DSWRF, by Lee et al. (2023) found a seasonally dependent mean bias of around +20 W m^{-2} during the winter, +40 W m^{-2} during the summer, and around +30 W m^{-2} in the spring during peak snow melt. The authors noted in the evaluation that these ranges are additionally dependent and vary with the amount of cloud cover, geographic region, ground cover type, and specific HRRR forecast hour. Keeping this high bias in mind, this study used the 6th-hour HRRR output, which showed a lower bias among all tested near surface product outputs and forecast hours. The use of DSWRF was additionally an opportunity to investigate a NWP

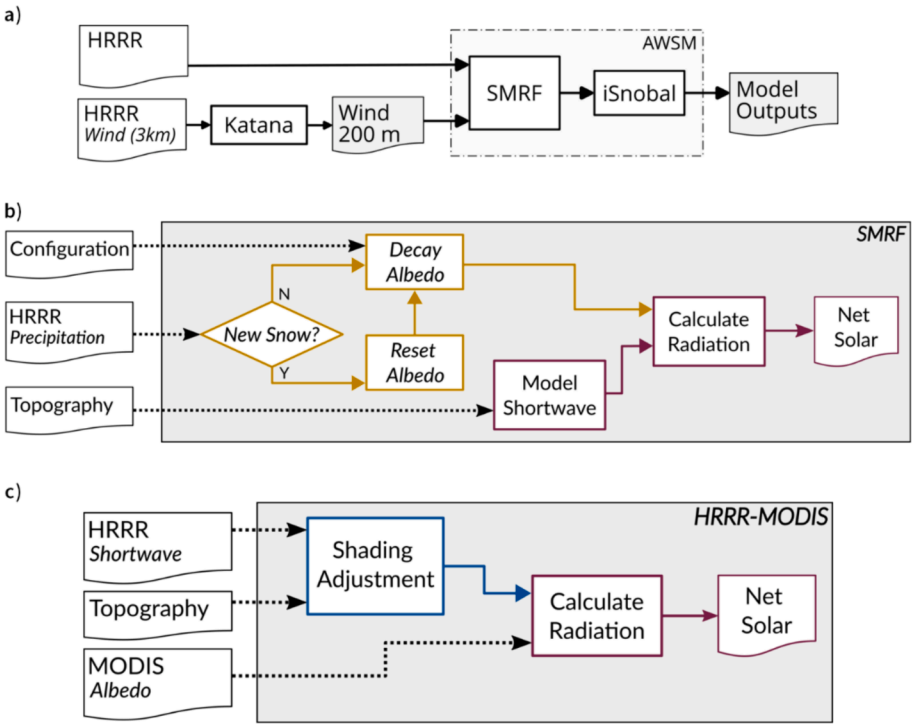

Fig. 3. Overview of the iSnobal architecture, input data, and execution workflow (a), the current net solar SMRF workflow (b), and the new implementation to calculate net solar using MODIS remotely sensed albedo and HRRR solar radiation (c).

radiation product, similar to Quéno et al. (2020), where spatially varying incoming solar radiation was better represented relative to empirical approaches. Adding a meteorological input from HRRR increased consistency among iSnobal forcing variables and reduced model design complexity of the HRRR-iSnobal combination. We note that for consistency in terminology, we use incoming solar radiation in place of DSWRF in this paper.

3.4. Albedo product

The MODIS snow albedo product used in this work is based on a combination of the MODSCAG and MODDRFS model outputs. MODSCAG uses a per-pixel spectral unmixing algorithm to detect snow, vegetation, rock, water, and shadow percentages. The spectral library for snow covers a range of snow grain sizes, which is the foundation for simultaneously detecting sub-pixel snow fraction and snow grain size (Painter et al., 2009). Using the spectral signature of the modeled clean snow grain size in MODSCAG and the information from the observed MODIS spectral information enables the MODDRFS algorithm to retrieve the reduction in visible albedo and radiative forcing impact of LAPs at the snow surface. Deriving broadband snow albedo with the information of both MODSCAG and MODDRFS was determined by Bair et al. (2019) to have a 4–6 % root means square error compared to a long-term in situ measurement record (4+ years). The albedo is gap-filled to be spatially and temporally complete (STC) through various filtering and smoothing techniques. The STC version of the MODIS snow retrievals improves fractional snow cover detection in forested areas, on cloudy days, and for varying satellite viewing geometry (Rittger et al., 2020). The MODIS snow property outputs are produced daily at 500 m spatial resolution keeping the MODIS Sinusoidal projection. Access to the data is provided upon request by the National Snow and Ice Data Center (NSIDC) Snow Today website (https://nsidc.org/reports/snow-today).

3.5. iSnobal net solar model process

3.5.1. Current implementation

Within the HRRR-iSnobal architecture, the current sole net solar radiation calculation option is available by SMRF and subsequently used as input to iSnobal (Fig. 3b). The two fundamental factors to this calculation (equation (1)) are the modeled time-decay snow albedo and the topographically adjusted incoming solar radiation. This process is simulated by SMRF at every user-configured time interval (1 h in this work) and stored as an input to iSnobal. The model configuration options and further process details for each factor are explained in the following sections.

3.5.1.1. Time-Decay snow albedo. For each model time step snow albedo is modeled using only the HRRR precipitation information with every new snowfall, above a user-defined threshold between time steps, restarting the decay. Aside from resetting the albedo, SMRF can accelerate the rate of albedo decay in the visible spectrum to account for LAPs using a 'dirt' factor parameter, which is applied between a user-configured start and end date. A common practice is to apply the faster decline during the ablation period, setting the dirt factor start date to the day of peak SWE and the end date to the last day with snow on the ground. An additional control on the decay rate is the vegetation type of a grid cell, where different rates are applied based on the type of cover. The vegetation type is retrieved from the metadata file (Fig. 1) created in the model domain preparation step. The last user-defined snow albedo influence factors are the maximum and minimum snow grain sizes to constrain changes in the near-infrared spectrum, which allow customizing the albedo decay for different snow environments. A detailed description of the time-decay albedo approach can be found in Marks and Dozier (1992).

3.5.1.2. Incoming solar radiation. Calculations for incoming solar radiation in SMRF use the algorithms presented in Dozier and Frew (1990). This approach starts with assuming a clear sky across the model domain and simplifying atmospheric influences. The required inputs are the model domain elevation data and the simulated day of year and time of day, which enables corrections due to topographic shading. Once the theoretical clear sky incoming solar radiation per grid cell is calculated, SMRF takes the HRRR solar radiation to determine a cloud reduction factor and reduces the clear sky value. The cloud reduction factor is the percentage of cloud cover and stored for further use within SMRF. The last step before the net solar calculation is the reduction due to vegetation cover, which is retrieved per grid cell from the modeled domain metadata. The motivation behind this approach was to resolve the incoming solar radiation at user-defined spatial resolutions, which may be finer than available incoming solar radiation data (Dozier and Frew, 1990). For example, HRRR values are at 3 km, and incoming solar radiation can exhibit variability at sub-kilometer scales in mountain topography.

3.5.2. New net solar implementation

Introducing the new option to the HRRR-iSnobal combination, to calculate net solar with the MODIS snow albedo product and HRRR solar radiation, was completed as an external set of forcing data preparation tools (Fig. 3c). Integrating the preparation tools into the iSnobal model workflow only required changes to SMRF. Here, the steps to calculate albedo and net solar were wrapped with a feature flag to disable the execution via the central model configuration file. The MODIS and HRRR product processing was performed in three steps and produced daily files with hourly resolution, which is the expected forcing input format by iSnobal.

First, the MODIS snow albedo product was cropped and reprojected to match the model domain in spatial projection (EPSG:32613), resolution, and extent. The spatial resampling used cubic interpolation to reduce observed artifacts within the albedo product, where neighboring pixels at times had large differences. These artifacts were deemed unrealistic and categorized as errors. To address the temporal resolution difference between set model simulation interval (1-hour) and MODIS product data (daily), the values of the daily MODIS overpass (around 10:30 AM MST) were used as the static snow albedo for the day. This approach does not represent albedo decay that happens over the day but rather the general daily patterns and magnitude of change over time. This approach may miss rapid changes as they happen, for example dust storms or new snow fall, but those would be captured with the next overpass on a clear cloud free day when impacts to albedo are most relevant for energy balance.

Then, the HRRR solar radiation values were cropped to the model domain and spatially resampled with the nearest neighbor algorithm to 50 m. HRRR data is available at hourly resolution and required no interpolation across time. Using the same approach as the current SMRF implementation to correct solar radiation values by a shading factor, the resampled HRRR values were adjusted by the model topography. The final step in creating the net solar input was multiplying the MODIS albedo with the topographically adjusted HRRR solar radiation on a pixel-by-pixel basis. The pixel-wise multiplication output was stored in the expected input format by iSnobal (daily files with hourly values).

Bypassing SMRF modeled solar also required an update to the cloud fraction estimation. In addition to scaling incoming clear sky solar radiation for cloud cover, SMRF also used cloud fraction to resolve longwave radiation fluxes. Consequently, the SMRF implementation was updated to use the HRRR cloud cover information to ensure identical forcing data across radiation calculations and consistency within the model framework.

4. Comparison

Assessment of the HRRR-iSnobal net solar radiation forcing updates

were performed in three stages. First, a run with the current time-decay snow albedo and the incoming solar radiation based on Dozier and Frew (1990) set the baseline to which the model modifications were compared to. These results are referred to as "Time-Decay". Next, the HRRR-iSnobal combination was updated to use the HRRR solar radiation and cloud cover data (label: HRRR-SC), with no updates to the treatment of albedo. The last run included the MODIS albedo product data along with the HRRR solar radiation and cloud cover data (label: HRRR-MODIS). The model outputs were assessed for each year in two ways; through time at discrete in situ observation points and across space at discrete points in time. The change in SWE over time, integrated across elevation bands, was also compared across model runs. These three categories are explained in the following sections.

4.1. Point comparison

Available observations at Irwin Study Plot (ISP) were compared to the energy balance model inputs to evaluate the forcing data quality. In addition to the meteorological measurements of air temperature, relative humidity, and wind speed/direction, the site has four separate pyranometers. The pyranometers are divided into pairs; two instruments measure the incoming and outgoing broadband solar radiation (Huskeflux SR-11; 0.285–2.800 μm) and the other two measure near-infrared solar radiation (Huskeflux SR-11, filtered; 0.695–2.800 μm), the difference of which is visible solar radiation. Broadband albedo was calculated by taking the ratio between outgoing and incoming solar radiation and then filtering to the closest time of MODIS overpass, a common practice for remote sensing assessments to local point observations (Sarangi et al., 2019; Bair et al., 2021). Computing net solar at ISP was derived from the difference between the incoming and outgoing broadband solar radiation (Wm^{-2}).

The HRRR-iSnobal output comparison values at ISP were retrieved from the corresponding 50-meter model grid cell containing the site when snow was present (snow depth > 0 m). The MODIS snow albedo and HRRR solar radiation were compared to ISP values over time and as a seasonal mean value. Net solar from the two updates were compared using the seasonal mean values and the median difference to the measured value. For assessment of HRRR air temperature and wind data, the observed values were subtracted from HRRR values, and a 1-day rolling mean was applied to reduce measurement spikes and compensate for data gaps.

Assessing the HRRR-iSnobal simulated snow depth values to the quality-controlled end-of-day measurements at the SNOTEL stations (Schofield Pass and Butte) used the grid cell encompassing the station's point location. This comparison first ensured that the model changes did not negatively impact the snow accumulation simulation, which was previously modeled well by HRRR-iSnobal (Meyer et al., 2023). Secondly, it evaluated the targeted improvements to snowmelt timing and snow disappearance dates through the incremental model changes.

A final evaluation of impacts to the forcing input changes with the snowpack energy balance calculation (equation (2)) compared the differences in the sum of energy (Q), net solar, net longwave, latent heat, and sensible heat at the two SNOTEL stations for each modification. The differences were calculated by subtracting the Time-Decay end-of-day values from HRRR-SC and HRRR-MODIS end-of-day values. The metrics included the seasonal mean, median, and standard deviation over the period where snow was present in the model grid cell containing the site.

4.2. Spatial comparison

A visual assessment across the ERW domain spot-checked the quality of the MODIS product and ensured that no widespread artifacts occurred, as occasionally seen in the initial evaluation. The selected date was April 1st, 2021, and marks the traditional day of peak SWE and the beginning of the melt season. Upon checking the Time-Decay results, this date also had a large spread for days since the last snowfall, making it a representative case where the albedo should vary across the model domain. To quantify the snow albedo variability, the mean and standard deviation were calculated and compared between the Time-Decay and MODIS product.

Assessing the propagation of net solar changes to model simulated snow depth across the ERW basin compared the model outputs against two aerial ASO lidar snow depth observations carried out in water year 2022 (no ASO flights occurred in 2021). The first flight was on the 21st of April and the second on the 18th of May. ASO data is publicly available via the NSIDC at 50 m spatial resolution. The objective was to evaluate how HRRR-MODIS changes impacted the snow depth simulations across the watershed while all other HRRR forcing input variables were held constant. The Time-Decay configuration previously simulated snow accumulation well with HRRR inputs (Meyer et al., 2023) and no degraded performance was anticipated.

In addition to the basin-wide snow depth comparison to ASO, the Time-Decay and HRRR-MODIS runs were compared in ASO observed snow-free areas (i.e., ASO grid cells with 0 m snow depth) to calculate the Snow Cover Extent (SCE) error. If snow melt was simulated too slowly, then the areas with snow depth in the model would be high, which would produce high SCE in this spatial comparison. Improvements to snow melt timing should reduce the SCE error, especially in the later flight when snowmelt was further underway. As an extension to this comparison the Time-Decay and HRRR-MODIS snow-free areas, not included with the previous case, were compared to observed depth by ASO (i.e. ASO grid cells with > 0 m snow depth). This inspected the model performance in areas where snowmelt occurred too quickly and causing SCE error.

4.3. Snow water equivalent

The changes to the HRRR-iSnobal net solar calculations were anticipated to propagate to SWE simulations and similarly follow the pattern of accelerated depletion during the melt season. The SWE inspection followed the classification from Meyer et al. (2023), where the elevation zones split the ERW watershed into a lower (< 2896 m/9500 ft), middle, and upper (> 3353 m/11 000 ft) elevation band (Fig. 1). Comparing the three zones summed the daily HRRR-iSnobal SWE outputs by the respective area. Similar to the spatial snow depth assessment, this comparison helped highlight whether model response to net solar updates varied across topography.

5. Results

5.1. Point comparison

5.1.1. Air temperature and wind speeds

The HRRR-iSnobal simulation assessment for air temperature and wind showed almost identical performance across both years at ISP (Fig. 4). For air temperature, the model forcing input had a difference spread relative to observations between $+4$ and -2 °C until December, at which the differences then started to fluctuate between $+4$ and -4 °C. Late in the melt season and starting around May, the temperatures were positively biased between 0 to $+4$ °C. The forcing inputs for wind showed no seasonal trends and difference values across both years stayed between $+2$ and -1 m/s. The close match between modeled forcing values and observed values gave confidence that the HRRR-iSnobal melt timing errors were primarily caused by errors in radiation as opposed to sensible or latent heat (turbulent fluxes).

5.1.2. Net solar

Compared to the measured net solar at ISP, the HRRR-MODIS and HRRR-SC configurations showed good agreement, with biases in incoming solar radiation and albedo balancing each other out (Fig. 5). For incoming solar radiation, the seasonal general trends were well represented, but values were consistently too high, especially

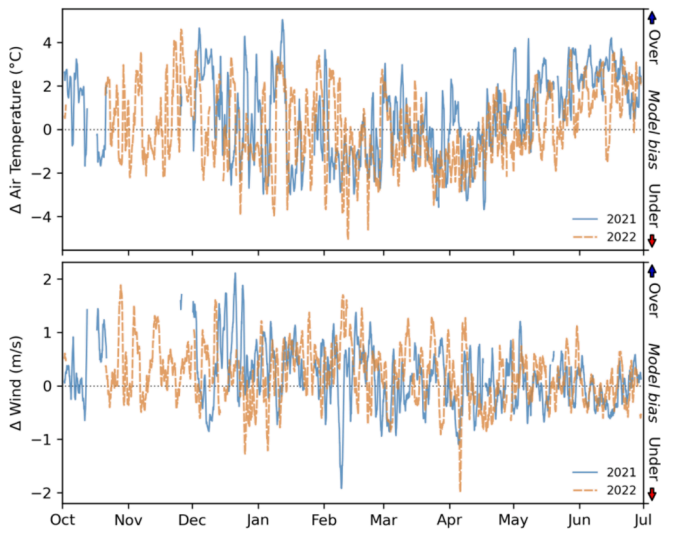

Fig. 4. HRRR-iSnobal simulation differences to Irwin Study Plot observations using a rolling 1-day moving mean for air temperature (top) and wind speeds (bottom). The gaps in the early season were caused by missing observation data.

pronounced in 2022 (Fig. 5 a, b). For albedo, there was more variability in the measurements relative to HRRR-SC (using Time-Decay albedo) and HRRR-MODIS (Fig. 5 c, d). The Time-Decay albedo was always too high, and the range of values too narrow, whereas MODIS better captured the general trends. The outcome for the model was a slight underestimation of net solar in both model configurations in 2021; −28 W m^{-2} (HRRR-SC) and −30 W m^{-2} (HRRR-MODIS) (Table 1). In 2022 HRRR-SC again underestimated (−28 W m^{-2}) whereas HRRR-MODIS overestimated net solar (+32 W m^{-2}). The best agreement in both water years was in the time period between December and the onset of melt (end of March) when the net solar difference between stayed between +/- 50 W m^{-2} (Fig. 5 e, f). Starting around the end of March, though, both model configurations had higher than observed net solar values. Getting the value closer to the observed is an area for future forcing product investigations and is discussed in section 6.2.

5.1.3. Energy balance terms

The simulated mean HRRR-iSnobal net solar radiation at the SNOTEL stations increased with each respective model change in both water years, showing the highest difference between the Time-Decay and HRRR-MODIS configuration (Fig. 6). Among the energy terms from equation (2), the net solar term had the largest changes. Here, the seasonal mean differences ranged from 11.8 W m^{-2} to 19.5 W m^{-2} in 2021 and 13.6 W m^{-2} to 32.4 W m^{-2} in 2022 at pixels containing the stations. This result confirmed the targeted increase of absorbed solar energy to improve the melt timings and magnitude. The second largest difference was with the net longwave term, where mean values ranged from −4.1 W/m^{-2} to −9.6 W m^{-2} in 2021 and −5.2 W m^{-2} to −16.2 W m^{-2} in 2022. This change is due to an increase in the snowpack temperature, caused by using a different cloud cover product and increased absorbed energy. Previous research analyzing model sensitivity to radiation energy inputs showed similar results, where changes to incoming longwave and shortwave propagated to snow temperature and therefore outgoing longwave energy (Lapo et al., 2015). A detailed overview with mean, standard deviation, and median values for net solar, net longwave, and sum of energy (Q) is given in Table 2.

5.1.4. Snow depth

Similar to net solar radiation, with each configuration update, the melt dates were simulated closer to observed (Fig. 7). The Time-Decay method lagged behind the observed SNOTEL station melt-out dates by 18 to 25 days at Butte and 15 to 33 days at Schofield Pass. The results from the HRRR-SC run reduced the difference to the observed at Butte to 3 to 8 days and at Schofield Pass from 2 to 12 days. Adding the MODIS product brought an additional reduction with the HRRR-MODIS run showing a difference of 1 to 6 days at Butte and 5 days at Schofield Pass. Schofield Pass was the only station in 2021, where the difference increased to 5 days with HRRR-MODIS versus 2 days with HRRR-SC (Table 3). For the season, the snow depth at each SNOTEL site was slightly reduced during the accumulation phase with HRRR-MODIS, especially when shallow snow depths (<0.2 m) were measured at the stations. Potential reasons for this are discussed in the "Limitations" section. Overall, using HRRR-MODIS as the net solar configuration produced the best result for simulated melt-out dates when compared to SNOTEL observations in the ERW domain across both years. These findings support the arguments of Meyer et al. (2023), where the net solar calculation of HRRR-iSnobal was suspected as the main contributor for the melt out simulation errors.

5.2. Spatial comparison

5.2.1. Albedo

Visually comparing the April 1st snow albedo between the Time-Decay method and the MODIS product showed that MODIS had lower values with higher spatial variability when the Time-Decay method showed almost no variation (Fig. 8). The mean Time-Decay albedo was 0.81 (SD of 0.01), while the MODIS product was 0.71 (SD of 0.07). The higher MODIS albedo variability and overall lower values were more realistic, given the time since snowfall was between 1 and 8 days. Using the MODIS product with HRRR-iSnobal also simulated less no snow areas at an identical point in time of the snow season between the Time-Decay and HRRR-MODIS configurations. As observed in the initial product assessment, the MODIS product had a few areas with lower than realistic albedo, which did not correspond to areas with no snow. These outliers could result from dense vegetation or low snowpack and are further discussed in the "Limitation" section.

5.2.2. Snow depth

Of the two ASO surveys in 2022, the late melt-season May flight showed a more noticeable improvement between HRRR-MODIS and ASO retrieved snow depth values at middle to lower elevations (Fig. 9). In April, the percentage of values in agreement (0.00 m depth difference) dropped slightly from the Time-Decay run (9.48%) to the HRRR-MODIS run (9.20%). The basin-wide difference changed from showing more areas with overestimation to having more underestimation, especially in the eastern portion of the ERW watershed boundaries. One month later, and further into the melt season, the HRRR-MODIS areas of agreement improved from 31.39% (Time-Decay) to 35.07%. The higher elevation showed a small change to having more snow with the HRRR-MODIS configuration. The general high underestimation for this elevation band and improvements for the HRRR-iSnobal combination are further discussed in section 6.4.

The SCE metric for April and before snowmelt had initiated was similar between configurations; 10.1% for Time-Decay and 12.7% for HRRR-MODIS (Fig. 10), showing little improvements to agreement in snow-free areas with ASO. For the May survey, when melt was progressing, the SCE error decreased from 13.4% (Time-Decay) to 3.2% (HRRR-MODIS). The increased snow-free agreement with the May survey confirmed watershed-wide snowmelt timing was improved using HRRR-MODIS. The comparison to assess potential drivers of too quickly melted out areas indicated tall vegetation as one of the main primary causes (Fig. 11). For the May 18th flight, the SCE error increased from 4.4% (Time-Decay) to 11.7% (HRRR-MODIS), which is further discussed in section 6.1.

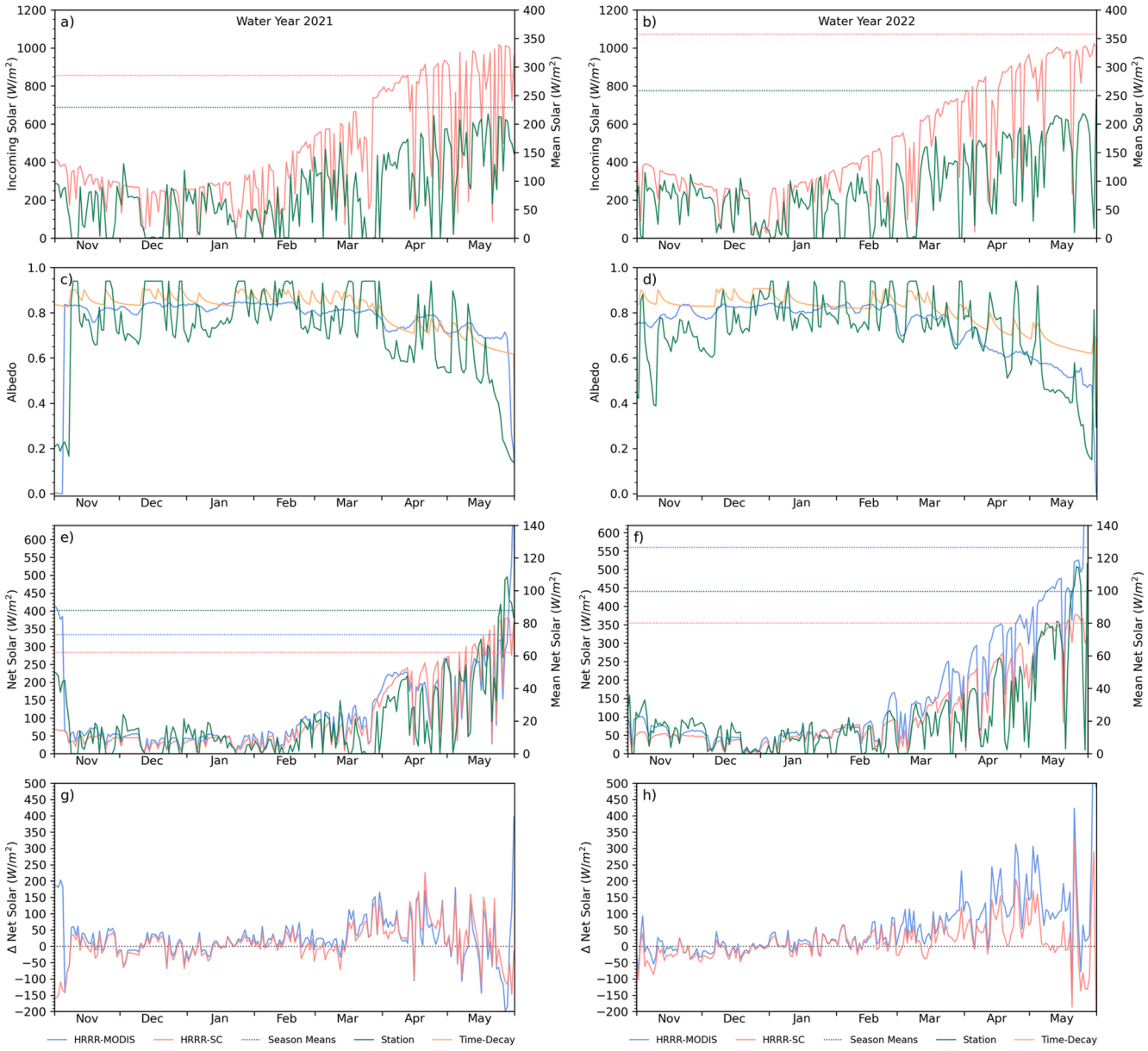

Fig. 5. Comparison of incoming solar (a, b), snow albedo (c, d), net solar (e, f), and the difference of simulated net solar to measured values (e, f) at the Irwin Study Plot for both simulated years.

Table 1
Overview of the net solar values for the HRRR-iSnobal configuration compared to measured Irwin Study Plot values, including the median differences across the two water years.

Irwin Study Plot	**Net Solar** (W m^{-2})	2021	2022
Mean	Station	88	99
	HRRR-SC	62	80
	HRRR-MODIS	73	126
Median Difference	HRRR-SC	−28	−28
	HRRR-MODIS	−30	32

5.3. *Snow water equivalent*

Across the three CBRFC elevation zones, the middle zone showed the biggest shift in the HRRR-MODIS configuration, with amount of total SWE depleting faster after the season peak was reached (Fig. 12). This change was observed for both water years and is consistent with the earlier HRRR-MODIS melt out dates at the SNOTEL stations, located in the middle zone. The SWE depletion also happened faster in the lower zone, although the difference was lower magnitude. At the highest elevations in the upper zone, though, HRRR-MODIS held SWE for longer and reduced snow slower than Time-Decay. This simulated SWE result matched the comparison with ASO snow depth, where the areas in the north higher elevation areas of the ERW watershed showed overestimation of snow depth in the HRRR-MODIS configuration. As a whole, the SWE comparison showed the expected propagation with earlier HRRR-MODIS melt dates in the lower and middle zone, depleting SWE faster and earlier than Time-Decay.

6. Discussion

6.1. *Propagation of model changes*

Each incremental change to the net solar calculation had a different impact on the observed versus simulated melt out date differences at the

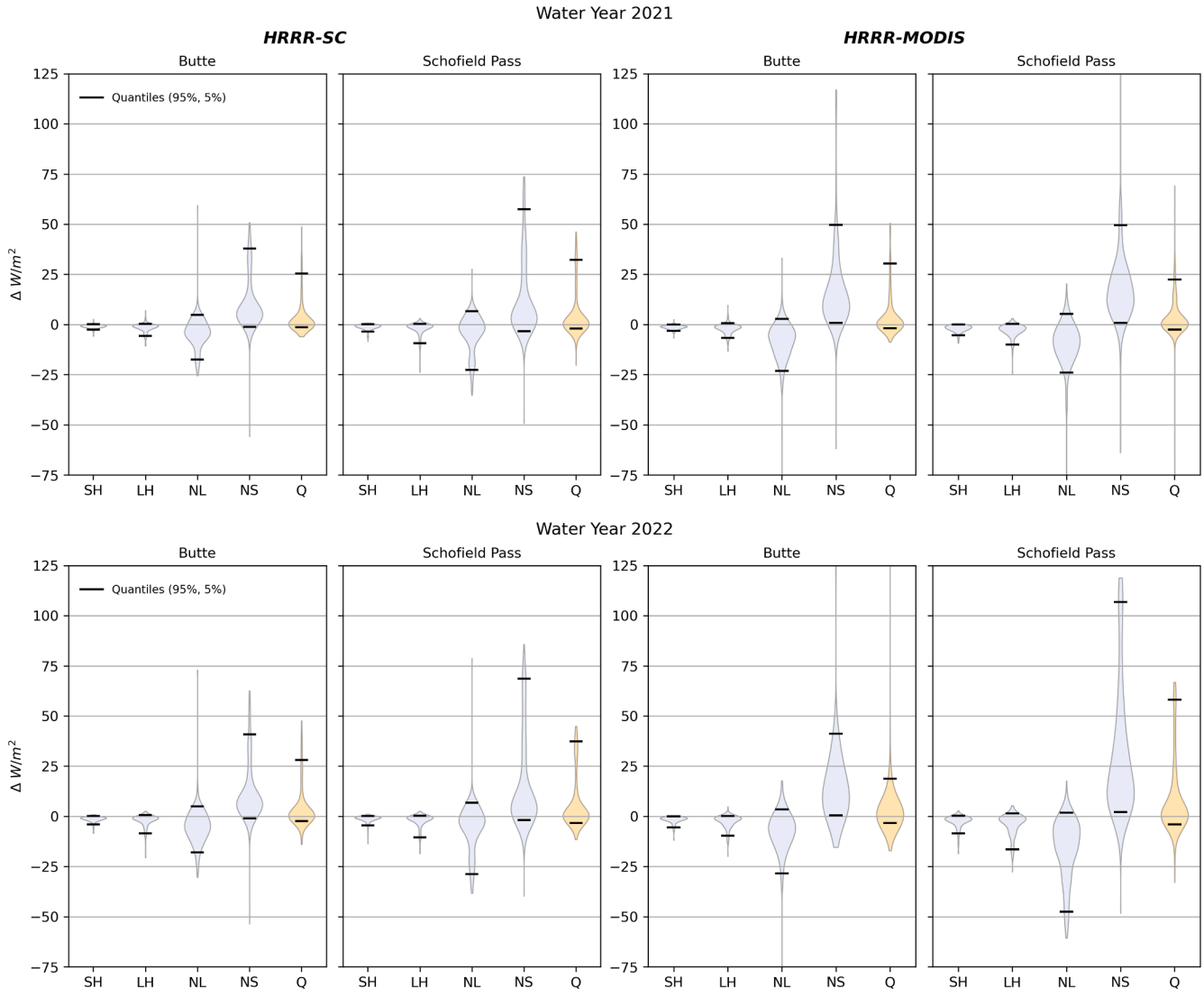

Fig. 6. Comparison of the changed energy fluxes with each model modification across each water year. Shown terms are Sensible Heat (SH), Latent Heat (LH), Net Longwave (NL), Net Solar (NS), and Sum of Energy (Q). Note that the Q-term also includes the ground-snow interfaces fluxes and advective energy from rain. These terms were excluded from the figure due to their small amount.

Table 2
Details of differences between net longwave (NL), net solar (NS), and sum of the energy terms (Q – Equation (2)) between the HRRR-SC and HRRR-MODIS model changes to the baseline Time-Decay run. The corresponding distributions are shown in Fig. 6.

Difference to Time-Decay (W m^{-2})			2021			2022		
			Mean	SD	Median	Mean	SD	Median
HRRR-SC	Butte	NL	−4.1	8	−3.8	−5.2	9.4	−5
		NS	11.8	12.1	6.4	13.6	13.8	7.8
		Q	3.6	8.8	0.3	4.2	10.5	0.5
	Schofield Pass	NL	−4.4	9.3	−2.4	−5.8	11.9	−3
		NS	15.7	18.5	5.7	19.4	22.8	6.3
		Q	4.7	11.1	0.4	6.2	12.8	0.3
HRRR-MODIS	Butte	NL	−8.7	10.9	−6.7	−9	14.9	−6.4
		NS	18.3	20	11.9	18.5	32.3	10.9
		Q	4.2	10	0.5	4.9	20.2	0.4
	Schofield Pass	NL	−9.6	12.2	−8.5	−16.2	14.9	−13.9
		NS	19.5	17.7	15.6	32.4	31.9	20.6
		Q	3.4	10.1	0.5	8.9	18.3	1

SNOTEL stations. Using the HRRR downward shortwave radiation product led to more available melt energy (Fig. 6) and consequently to earlier melt out dates, reducing the difference to the observed by over 10 days for each water year and station (Table 3). Additionally replacing the time-decay with MODIS albedo product lowered this by a couple more days, making it seem less of an important factor at first. However, the two point comparisons in combination with the basin-wide improvements to snow free areas late in the melt season agreement (from

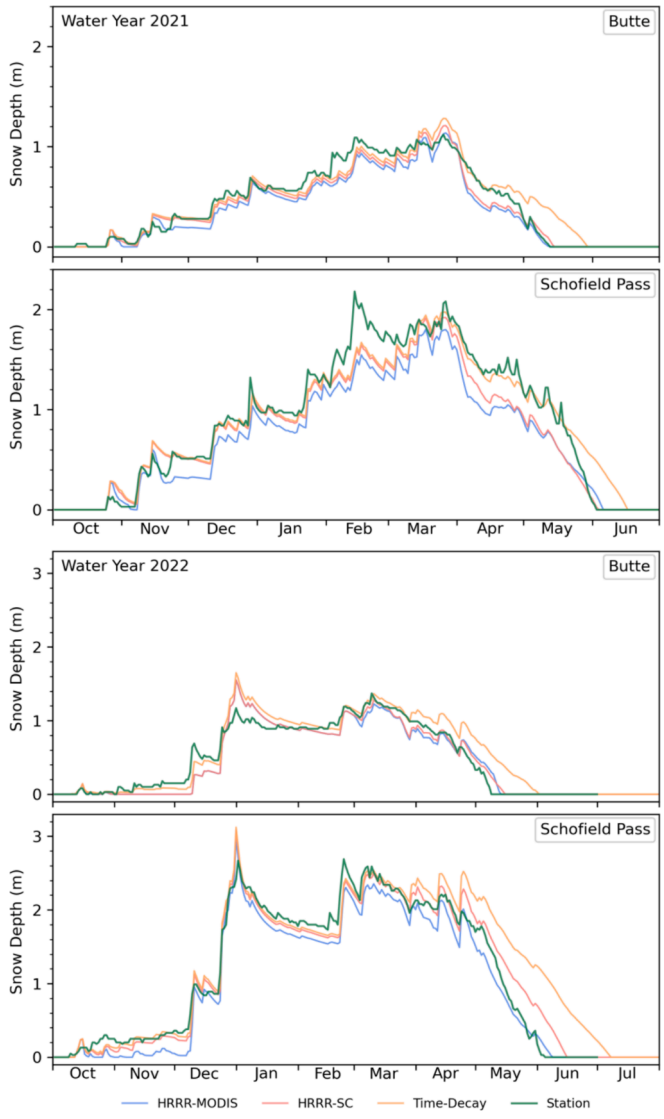

Fig. 7. Simulated snow depth comparison across the model modifications, water years, and against the observed SNOTEL site depth. Note the different y scale between the two water years.

Table 3
Overview of simulated HRRR-iSnobal melt out dates across the different net solar methods compared to the SNOTEL station observed date.

SNOTEL site	**Melt out dates**	2021	2022
Butte	Station	12-May	2-Jun
	Time-Decay	+18 days	+25 days
	HRRR-SC	+3 days	+8 days
	HRRR-MODIS	+1 day	+6 days
Schofield Pass	Station	2-Jun	4-Jun
	Time-Decay	+15 days	+33 days
	HRRR-SC	+2 days	+12 days
	HRRR-MODIS	+5 days	+5 days

87 % to 97 %, Fig. 10) make the case that both changes to the net solar calculation inputs were needed to get closest to the observed. This need is additionally backed up when looking at the differences to the net solar energy term with each iteration (Table 2), where the amount increased each time and causing more available melt energy. A more basin-wide melt date impact analysis, through modifications to either the incoming shortwave radiation, the observed albedo, or both, would require more in-situ measurement stations or higher frequency areal snow depth observations, which were not available at the time of this study. Applying this incremental iSnobal net solar calculation update in other areas where more in-situ or spatial observations are available can further assess if the melt out date improvement hold true across a wider range of watersheds.

6.2. *MODIS snow product considerations*

The MODIS product derives snow albedo using a threshold for snow-covered area per pixel (>90 %), which limits accurate retrievals under certain conditions. For instance, increased gaps in observed snow cover can be caused by tall vegetation, where the product is known to have lower than observed albedo (Stillinger et al., 2023). This effect was found in this study in the spatial comparison, where the eastern side of the ERW domain with tall vegetation changed to more areas of model underestimated snow depth (Fig. 11). However, this change can also stem from a need to further correct the HRRR solar radiation with influences from the terrain or to revise the vegetation representation in iSnobal. Similar strong vegetation influences in the ERW was also found by Feldman et al. (2022). Ultimately, the newly highlighted underperformed regions in the study domain are the basis for future analysis of the MODIS product, HRRR solar radiation, or the energy balance calculation in iSnobal.

Additional conditions where satellite-based products underestimate the albedo are shallow or patchy snow cover. Shallow snow depths are impacted by the underlying substrate of the snow as the light penetrates down to the ground, causing the snow to appear darker. Inconsistent snow cover throughout a MODIS scene or within a single pixel result in more pixels being excluded from the retrieval algorithm, increasing the need to interpolate. The shallow snow depth case was observed in this study, especially at the beginning of 2022 at Schofield Pass (Fig. 6), where HRRR-MODIS had lower simulated grid-cell snow depth from October to December when depths fell below 0.2 m. A similar snow depth threshold with a point comparison was observed in Bair et al. (2022) and the authors limited their MODIS albedo quality assessment to depths above 0.2 m.

The HRRR-MODIS configuration did not deplete SWE as fast in the higher elevations (> 11 000 ft) during the melt season, contrary to expectations and results in the lower and middle elevations (Fig. 12). Reasons for holding snow longer could be due to undetected clouds in the MODIS product leading to higher albedo values (Rittger et al., 2020) and therefore lower net solar values. Additionally, the HRRR-supplied solar radiation also contributes to this issue having the average elevation per 3-km grid cell (Dowell et al., 2022), flattening out high peaks, and producing lower values. However, this change at higher elevations will require further analysis as HRRR-iSnobal underperforms in this zone (Meyer et al., 2023) and remains an active research area for model advances.

6.3. *Temporal and spatial data resolutions*

Replacing the theoretical snow albedo approach and using a spatially and temporally gap-filled remotely sensed product along with a relatively coarse spatial (3 km) but high temporal resolution HRRR solar radiation product improved the models' snow energy balance calculation. This input data source combination was tested in this work across a large domain (1300 km^2) at 50 m spatial resolution and daily outputs over two waters years. With these inputs, HRRR-MODIS showed little degradation during the accumulation season at lower or middle elevations, as seen with the SNOTEL results (Fig. 7). The objective of this effort, to produce a better match between simulated and observed snowmelt timing was achieved (Fig. 10), despite the present biases in each product compensating the effects of too high albedo and too high incoming solar radiation (and combinations thereof). The bias in HRRR solar radiation was deemed reasonable, especially when relating to similar findings by Hinkelman et al. (2015) and Quéno et al. (2020),

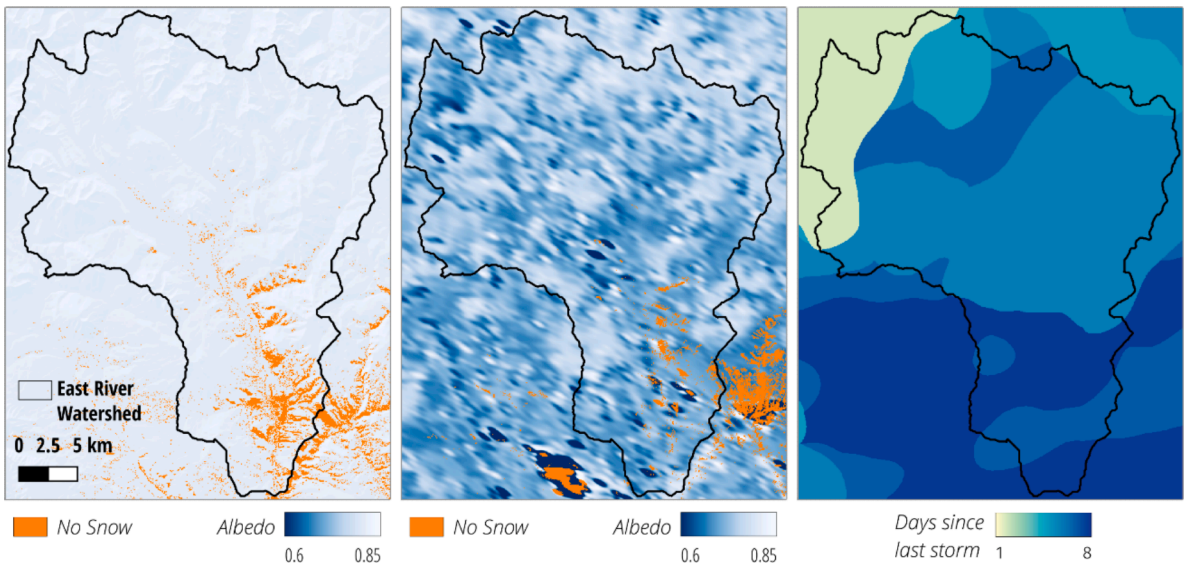

Fig. 8. Areal comparison of simulated Time-Decay snow albedo values (left) to MODIS product values (center), and map with elapsed days since last snowfall (right) on April 1st, 2021. The map with elapsed days since snowfall is an input product to the Time-Decay method in SMRF. Note the identical color scale for the albedo values (left and center).

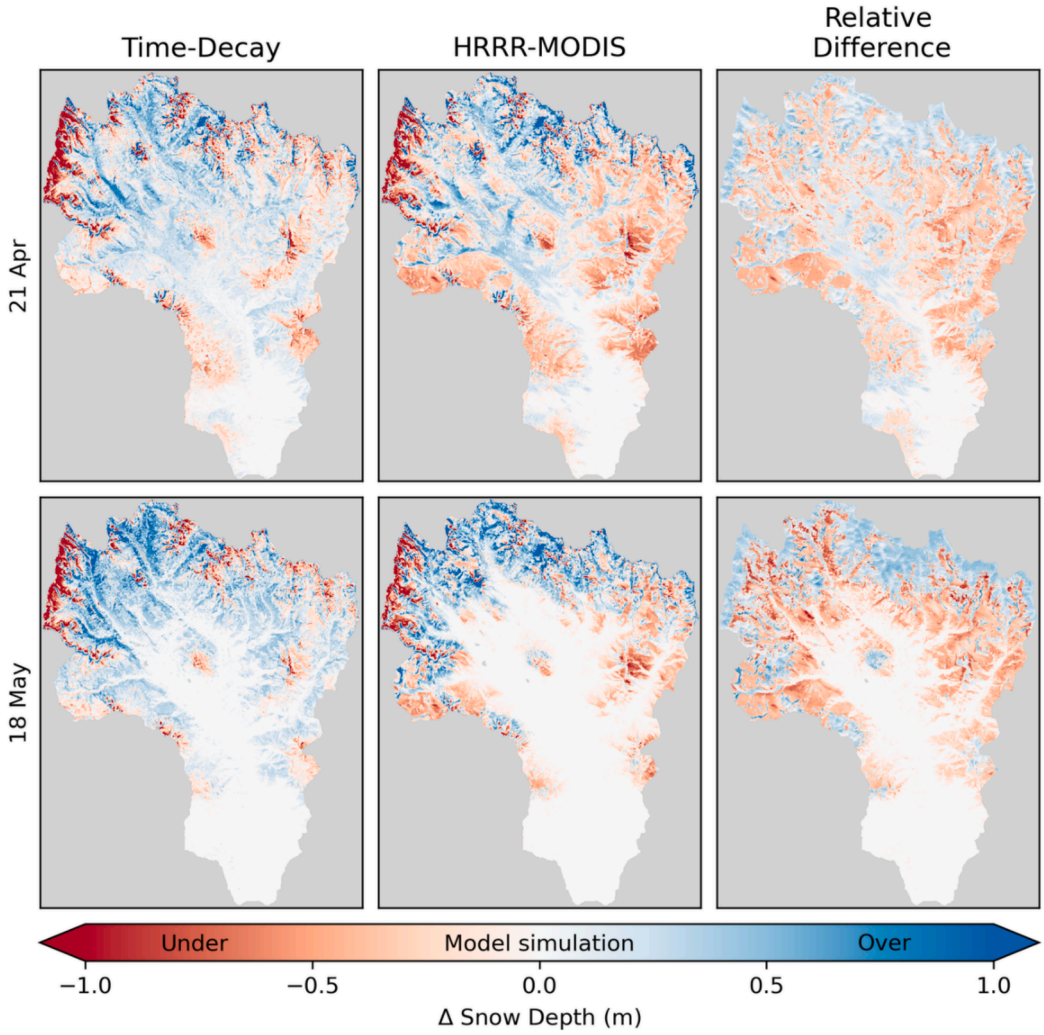

Fig. 9. Areal maps of the snow depths differences between Time-Decay and HRRR-MODIS simulated to ASO measured values in 2022. The differences were calculated by subtracting the ASO depths from the model depths. The "Relative Differences" were calculated by subtracting the Time-Decay from the HRRR-MODIS differences.

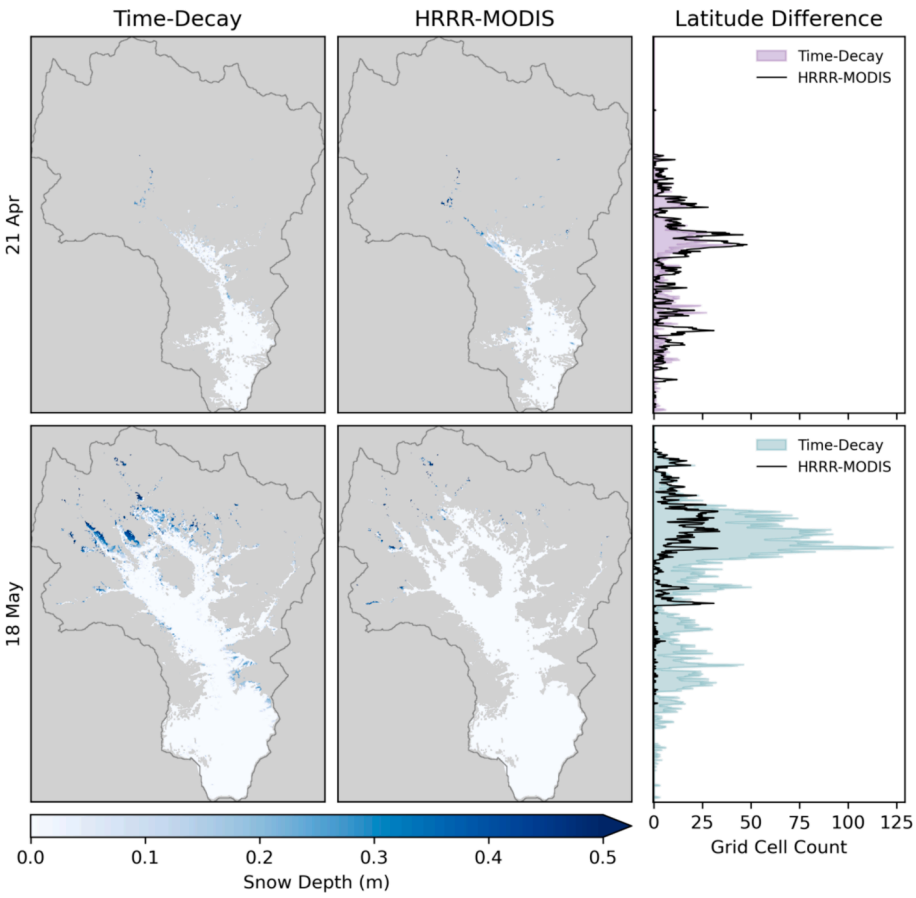

Fig. 10. Comparison of snow depth from the Time-Decay and HRRR-MODIS configurations within the snow free area measured by ASO. For comparison, the distribution plots on the right counted the number of grid cells with simulated snow depth along the ERW latitude from South to North.

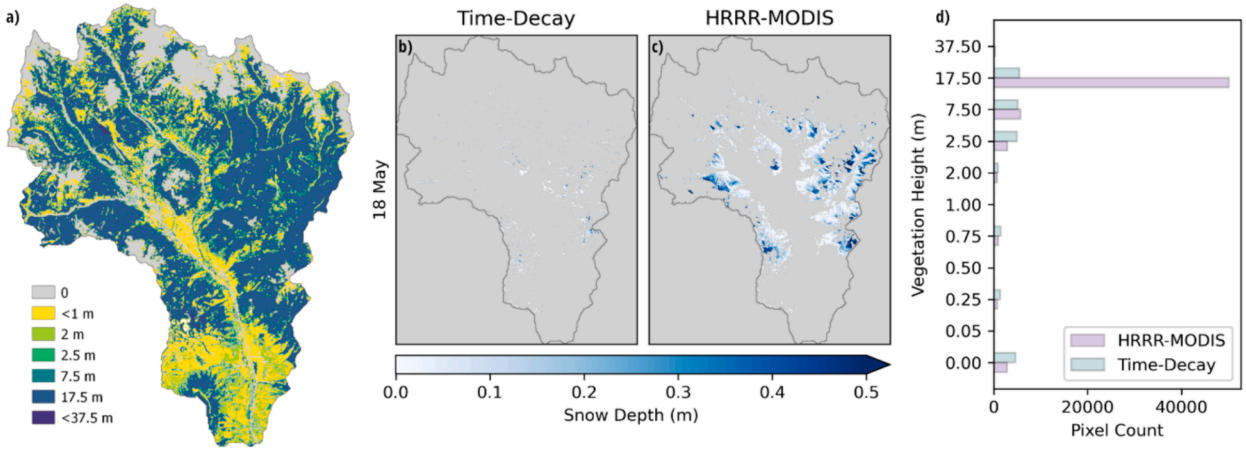

Fig. 11. Model performance on May 18th showing pixels with measured snow depth (snow > 0 m) by ASO, but simulated snow-free areas (snow = 0 m) in Time-Decay (b) and HRRR-MODIS (c) runs. The vegetation height distribution of the corresponding pixels in (b) and (c) is shown in (d), with the ERW vegetation height map for reference in (a).

where snow models performed favorably when forced by NWP radiation or satellite-based products. Providing accurate simulated or retrieved solar radiation products across space and time in the mountains remains a challenge due to the large uncertainties caused by rapidly changing topography and weather conditions across seasons (Lapo et al., 2017).

6.4. *Revised snow albedo representation*

With the two-layer snowpack architecture, the iSnobal model uses the top layer to interact with the atmosphere. Therefore, the best option to advance the model's inclusion of spatially varying LAP deposition and albedo decay from the current basin-wide identical time decay was to use remotely sensed snow surface albedo as confirmed with the April 1st comparison (Fig. 8). The observed albedo additionally integrated the

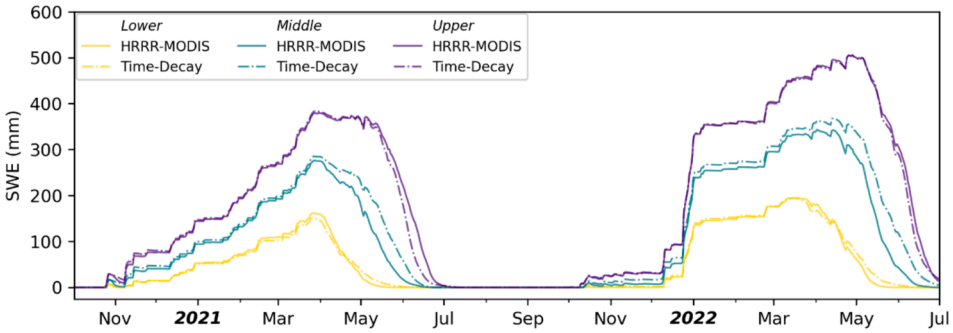

Fig. 12. Time-Decay and HRRR-MODIS SWE comparison for the two simulated water years. The lower, middle, and upper zone categorization is by elevation and taken from the Colorado Basin River Forecast Center operational division.

accumulative effects of multiple LAP depositions in the snowpack as they propagated to the surface during melt (Skiles et al., 2012). The resulting reduction is considered the direct effect (Skiles and Painter, 2019; Tuzet et al., 2017) and has been shown to change the radiative energy of snow energy balance calculations between 80 % (Skiles and Painter, 2019) and 85 % (Tuzet et al., 2017). The observed albedo also combined the different effects of the LAP mixing state (Liou et al., 2014; He et al., 2014), indirectly including other LAP snow-darkening aspects.

This presented direct insertion of snow albedo can replace the various time-based surface aging approach with any spatially distributed or point model architecture that accounts for albedo changes. For instance, all the investigated physical based snow models (e.g. Crocus, SNOWPACK, or SMAP) in Krinner et al. (2018) would benefit from using this snow albedo replacement, addressing the identified model melt timing shortcomings. Care must be taken however on how a change in surface energy will affect the snowpack dynamics. Depending on the number of layers represented in each model, the resulting difference in energy will propagate differently to the other energy terms such as the net longwave (Lapo et al., 2015).

6.5. Further HRRR-iSnobal work

This first iteration of using remote sensing values with the HRRR-iSnobal combination improved the simulated melt processes, and there are several options to increase the accuracy further. For instance, the HRRR solar radiation could be refined by applying sub-grid variability corrections, as shown by He et al. (2019). Improving pixel-wise algorithms through other means than increasing the spatial resolution has been successfully applied to snow processes in large-scale models (Smirnova et al., 2016) and kept the added computational overhead low. Other topographic-related enhancement options include ray tracing-based models for shading and clear-sky corrections that can include influences of reflected solar radiation by surrounding terrain (Steger et al., 2022). Additional possible follow-up efforts to this work are an in-depth model performance and sensitivity analysis to the snow energy balance calculations based on the in situ records from the Surface Atmosphere Integrated Field Laboratory (SAIL; Feldman et al., 2023) and Study of Precipitation, the Lower Atmosphere and Surface for Hydrometeorology (SPLASH; https://gml.noaa.gov/grad/splash.html) campaigns. Both efforts (SAIL and SPLASH) include extensive observations of surface energy balance components including wind, cloud cover, and radiation observations at strategic point locations in the ERW basin over a two year period. This data source did not overlap with the available MODIS product time record at the time of conducting this study.

A remaining continued investigation for the HRRR-iSnobal combination is the large depth underestimation at higher elevations in the north and north-western ERW region (Fig. 9). This model underperformance was identified in Meyer et al. (2023) as a HRRR precipitation forcing input issue, flattening out tall peaks from the topography and having sparse data observations for HRRR model initialization. From an operational forecasting application perspective, the presented option for HRRR-iSnobal needs further refinement to adapt other sources than the MODIS product and increased automation of the direct insertion method. Creating a more robust and flexible workflow will increase the future application of this method and help transition as the default snow albedo model representation.

7. Conclusion

A new option to determine the net solar radiation in the HRRR-iSnobal combination was presented and advanced the snow albedo representation by using observations from a remote sensing product. The combination of MODIS-derived albedo plus NWP-modeled incoming solar radiation improved the HRRR-iSnobal simulated melt-out dates within one to six days compared to in situ point observations. There was a seasonal net solar median difference of 25 W m^{-2} and 27 W m^{-2} relative to in situ observations, an improvement over Time-Decay differences of 109 W m^{-2} and 110 W m^{-2}. Higher net solar radiation accelerated modeled snowmelt, bringing snow depth depletion rates and timing closer in line with observations. Additionally, this improved modeled snow extent; the agreement between the model and observations in the late melt-season showed an improvement in snow depleted areas from 86.6 % (Time-Decay) to 96.8 % (HRRR-MODIS). The advanced melt timings were also reflected in the SWE outputs, releasing snow melt water earlier.

Alongside the improvements, though, the results also highlighted areas for further research. For the MODIS product, snow melt timing results suggest albedo values were underestimated in areas of tall vegetation and overestimated at higher elevations. The HRRR supplied incoming solar radiation compared high against an in situ point observation. Outcomes of the spatial and point comparison also suggested revisiting the representation of vegetation and an investigation into higher elevation performance for the HRRR-iSnobal combination. Based on the overall results and significant improvement in snowmelt timing, though, we propose replacing the time-decay snow albedo in iSnobal with the remote sensing data and NWP incoming solar radiation as the default method going forward. Although there is risk associated with this approach given that MODIS is near end of life, it is likely gaps will be filled by the snow products currently undergoing assessment from VIIRS (Rittger et al., 2021, Stillinger et al., 2023). Additionally, future imaging spectroscopy missions, such as Surface Biology and Geology by the National Aeronautics and Space Administration agency (NASA SBG; Cawse-Nicholson et al., 2021), will support the incorporation of snow albedo into models as it is one of the designated observables. Other satellite missions, such as the Copernicus Hyperspectral Imaging Mission for the Environment by the European Space Agency (ESA CHIME; Rast et al., 2021) or Planet Tanager may also assist in providing the required remote sensing observations.

Code availability.

The software components used to run the model and analyze the

results are publicly available. iSnobal model components are available via the USDA ARS NWRC GitHub page: https://github.com/USDA-ARS-NWRC. Additions to model setup and result analysis code are stored on the University of Utah GitHub organization repository: https://github.com/UofU-Cryosphere/isnoda (https://doi.org/10.5281/zenodo.11245701).

Data availability.

The following datasets were used for the model runs and comparisons:

- The National Elevation Dataset (NED), U.S. Department of the Interior, Geological Survey https://apps.nationalmap.gov/viewer/
- LANDFIRE, 2014, Existing Vegetation Type and Height Layer, LANDFIRE 1.4.0, U.S. Department of the Interior, Geological Survey, and U.S. Department of AgricultureData Product Mosaic Downloads: https://landfire.gov/getdata.php
- NOAA The High-Resolution Rapid Refresh (HRRR): https://rapidrefresh.noaa.gov/hrrr/
- NRCS National Water and Climate Center | SNOTEL | SWE Data: https://www.wcc.nrcs.usda.gov/snow/SNOTEL-wedata.html
- The National Map | U.S. Geological Survey: https://www.usgs.gov/programs/national-geospatial-program/national-map
- USGS Surface Water data for USA: USGS Surface-Water Daily Statistics: https://waterdata.usgs.gov/nwis/dvstat/?site_no = 09112500&referred_module = sw&format = sites_selection_links
- Painter, T. H.: ASO L4 Lidar Snow Depth 50 m UTM Grid, Version 1. [USCOGE]. Boulder, Colorado USA. NASA National Snow and Ice Data Center Distributed Active Archive Center, NSIDC, https://doi.org/10.5067/STOT5I0U1WVI, 2018
- STC MODIS product from the National Snow and Ice Data Center: https://nsidc.org/snow-today

Author contributions.

JM and MS conceptualized the overall study, with helpful contributions from all authors. JM performed the model runs and analysis. JM wrote the first draft of the manuscript, which was then contributed to by all authors.

CRediT authorship contribution statement

Joachim Meyer: Writing – review & editing, Writing – original draft, Methodology, Investigation, Formal analysis, Data curation, Conceptualization. **Andrew Hedrick:** Writing – review & editing, Methodology, Conceptualization. **S. McKenzie Skiles:** Writing – review & editing, Project administration, Methodology, Funding acquisition, Conceptualization.

Declaration of competing interest

The authors declare that they have no known competing financial interests or personal relationships that could have appeared to influence the work reported in this paper.

Data availability

All data access is listed under “Data availability”

Acknowledgements

The authors would like to thank Karl Rittger and the team at SnowToday for providing support and early access to the STC MODIS product. The support and resources from the Center for High Performance Computing (CHPC) at the University of Utah are gratefully acknowledged.

This work was funded by the NASA ESD Applied Sciences - Water Resources (grant number 80NSSC19K1243) and by NOAA via the Cooperative Institute for Research on Hydrology (CIROH) (grant number NA22NWS4320003).

References

Abolafia-Rosenzweig, R., He, C., McKenzie Skiles, S., Chen, F., Gochis, D., 2022. Evaluation and Optimization of Snow Albedo Scheme in Noah-MP Land Surface Model Using In Situ Spectral Observations in the Colorado Rockies. J Adv Model Earth Syst 14. https://doi.org/10.1029/2022MS003141.

Aoki, T., Kuchiki, K., Niwano, M., Kodama, Y., Hosaka, M., Tanaka, T., 2011. Physically based snow albedo model for calculating broadband albedos and the solar heating profile in snowpack for general circulation models. J. Geophys. Res. 116, D11114. https://doi.org/10.1029/2010JD015507.

Bair, E.H., Rittger, K., Skiles, S.M., Dozier, J., 2019. An Examination of Snow Albedo Estimates From MODIS and Their Impact on Snow Water Equivalent Reconstruction. Water Resources Research 55, 7826–7842. https://doi.org/10.1029/2019WR024810.

Bair, E.H., Stillinger, T., Dozier, J., 2021. Snow Property Inversion From Remote Sensing (SPIReS): A Generalized Multispectral Unmixing Approach With Examples From MODIS and Landsat 8 OLI. IEEE Trans. Geosci. Remote Sensing 59, 7270–7284. https://doi.org/10.1109/TGRS.2020.3040328.

Bair, E.H., Dozier, J., Stern, C., LeWinter, A., Rittger, K., Savagian, A., Stillinger, T., Davis, R.E., 2022. Divergence of apparent and intrinsic snow albedo over a season at a sub-alpine site with implications for remote sensing. The Cryosphere 16, 1765–1778. https://doi.org/10.5194/tc-16-1765-2022.

Bartelt, P., Lehning, M., 2002. A physical SNOWPACK model for the Swiss avalanche warning: Part I: numerical model. Cold Regions Science and Technology 35, 123–145. https://doi.org/10.1016/S0165-232X(02)00074-5.

Bonnell, R., McGrath, D., Hedrick, A.R., Trujillo, E., Meehan, T.G., Williams, K., Marshall, H.P., Sexstone, G., Fulton, J., Ronayne, M.J., Fassnacht, S.R., Webb, R.W., Hale, K.E., 2023. Snowpack relative permittivity and density derived from near-coincident lidar and ground-penetrating radar. Hydrological Processes 37 (10), 1–17. https://doi.org/10.1002/hyp.14996.

Cawse-Nicholson, K., Townsend, P.A., Schimel, D., Assiri, A.M., Blake, P.L., Buongiorno, M.F., Campbell, P., Carmon, N., Casey, K.A., Correa-Pabón, R.E., Dahlin, K.M., Dashti, H., Dennison, P.E., Dierssen, H., Erickson, A., Fisher, J.B., Frouin, R., Gatebe, C.K., Gholizadeh, H., Gierach, M., Glenn, N.F., Goodman, J.A., Griffith, D.M., Guild, L., Hakkenberg, C.R., Hochberg, E.J., Holmes, T.R.H., Hu, C., Hulley, G., Huemmrich, K.F., Kudela, R.M., Kokaly, R.F., Lee, C.M., Martin, R., Miller, C.E., Moses, W.J., Muller-Karger, F.E., Ortiz, J.D., Otis, D.B., Pahlevan, N., Painter, T.H., Pavlick, R., Poulter, B., Qi, Y., Realmuto, V.J., Roberts, D., Schaepman, M.E., Schneider, F.D., Schwandner, F.M., Serbin, S.P., Shiklomanov, A. N., Stavros, E.N., Thompson, D.R., Torres-Perez, J.L., Turpie, K.R., Tzortziou, M., Ustin, S., Yu, Q., Yusup, Y., Zhang, Q., 2021. NASA's surface biology and geology designated observable: A perspective on surface imaging algorithms. Remote Sensing of Environment 257, 112349. https://doi.org/10.1016/j.rse.2021.112349.

Chen, F., Barlage, M., Tewari, M., Rasmussen, R., Jin, J., Lettenmaier, D., Livneh, B., Lin, C., Miguez-Macho, G., Niu, G.-Y., Wen, L., Yang, Z.-L., 2014. Modeling seasonal snowpack evolution in the complex terrain and forested Colorado Headwaters region: A model intercomparison study. J. Geophys. Res. Atmos. 119, 13795–13819. https://doi.org/10.1002/2014JD022167.

Clark, M.P., Nijssen, B., Lundquist, J.D., Kavetski, D., Rupp, D.E., Woods, R.A., Freer, J. E., Gutmann, E.D., Wood, A.W., Gochis, D.J., Rasmussen, R.M., Tarboton, D.G., Mahat, V., Flerchinger, G.N., Marks, D.G., 2015. A unified approach for process-based hydrologic modeling: 2. Model implementation and case studies. Water Resources Research 51, 2515–2542. https://doi.org/10.1002/2015WR017200.

DeWalle, D.R., Rango, A., 2008. Principles of Snow Hydrology. Cambridge University Press, Cambridge. https://doi.org/10.1017/CBO9780511535673.

Donahue, C., Skiles, S.M., Hammonds, K., 2021. In situ effective snow grain size mapping using a compact hyperspectral imager. Journal of Glaciology 67, 49–57. https://doi.org/10.1017/jog.2020.68.

Dowell, D.C., Alexander, C.R., James, E.P., Weygandt, S.S., Benjamin, S.G., Manikin, G. S., Blake, B.T., Brown, J.M., Olson, J.B., Hu, M., Smirnova, T.G., Ladwig, T., Kenyon, J.S., Ahmadov, R., Turner, D.D., Duda, J.D., Alcott, T.I., 2022. The High-Resolution Rapid Refresh (HRRR): An Hourly Updating Convection-Allowing Forecast Model. Part I: Motivation and System Description. Weather and Forecasting 37, 1371–1395. https://doi.org/10.1175/WAF-D-21-0151.1.

Dozier, J., Frew, J., 1990. Rapid calculation of terrain parameters for radiation modeling from digital elevation data. IEEE Transactions on Geoscience and Remote Sensing 28, 963–969. https://doi.org/10.1109/36.58986.

Ek, M.B., Mitchell, K.E., Lin, Y., Rogers, E., Grunmann, P., Koren, V., Gayno, G., Tarpley, J.D., 2003. Implementation of Noah land surface model advances in the National Centers for Environmental Prediction operational mesoscale Eta model. Journal of Geophysical Research: Atmospheres 108. https://doi.org/10.1029/2002JD003296.

Feldman, D.R., Worden, M., Falco, N., Dennedy-Frank, P.J., Chen, J., Dafflon, B., Wainwright, H., 2022. Three-Dimensional Surface Downwelling Longwave Radiation Clear-Sky Effects in the Upper Colorado River Basin. Geophysical Research Letters 49, e2021G–L094605. https://doi.org/10.1029/2021GL094605.

Feldman, D. R., Aiken, A. C., Boos, W. R., Carroll, R. W. H., Chandrasekar, V., Collis, S., Creamean, J. M., Boer, G. de, Deems, J., DeMott, P. J., Fan, J., Flores, A. N., Gochis, D., Grover, M., Hill, T. C. J., Hodshire, A., Hulm, E., Hume, C. C., Jackson, R., Junyent, F., Kennedy, A., Kumjian, M., Levin, E. J. T., Lundquist, J. D., O'Brien, J., Raleigh, M. S., Reithel, J., Rhoades, A., Rittger, K., Rudisill, W., Sherman, Z., Siirila-Woodburn, E., Skiles, S. M., Smith, J. N., Sullivan, R. C., Theisen, A., Tuftedal, M.,

Varble, A. C., Wiedlea, A., Wielandt, S., Williams, K., and Xu, Z.: The Surface Atmosphere Integrated Field Laboratory (SAIL) Campaign, Bulletin of the American Meteorological Society, 104, E2192–E2222, https://doi.org/10.1175/BAMS-D-22-0049.1, 2023.

Forthofer, J.M., Butler, B.W., Wagenbrenner, N.S., Forthofer, J.M., Butler, B.W., Wagenbrenner, N.S., 2014. A comparison of three approaches for simulating fine-scale surface winds in support of wildland fire management. Part I. Model formulation and comparison against measurements. Int. J. Wildland Fire 23, 969–981. https://doi.org/10.1071/WF12089.

Gardner, A.S., Sharp, M.J., 2010. A review of snow and ice albedo and the development of a new physically based broadband albedo parameterization. J. Geophys. Res. 115, F01009. https://doi.org/10.1029/2009JF001444.

Garen, D.C., Marks, D., 2005. Spatially distributed energy balance snowmelt modelling in a mountainous river basin: estimation of meteorological inputs and verification of model results. Journal of Hydrology 315 (1–4), 126–153. https://doi.org/10.1016/j.jhydrol.2005.03.026.

Hale, K., Kiewiet, L., Trujillo, E., Krohe, C., Hedrick, A.R., Marks, D., Kormos, P.R., Havens, S., McNamara, J., Link, T., Godsey, S.E., 2023. Drivers of spatiotemporal patterns of surface water inputs in a catchment at the rain-snow transition zone of the water-limited western United States. Journal of Hydrology 616 (October 2022). https://doi.org/10.1016/j.jhydrol.2022.128699.

Hao, D., Bisht, G., Rittger, K., Stillinger, T., Bair, E., Gu, Y., Leung, L.R., 2022. Evaluation of snow processes over the Western United States in E3SM land model. Egusphere 1–38. https://doi.org/10.5194/egusphere-2022-1097.

Havens, S., Marks, D., Kormos, P., Hedrick, A., 2017. Spatial Modeling for Resources Framework (SMRF): A modular framework for developing spatial forcing data for snow modeling in mountain basins. Computers & Geosciences 109, 295–304. https://doi.org/10.1016/j.cageo.2017.08.016.

Havens, S., Marks, D., Sandusky, M., Hedrick, A., Johnson, M., Robertson, M., Trujillo, E., 2020. Automated Water Supply Model (AWSM): Streamlining and standardizing application of a physically based snow model for water resources and reproducible science. Computers & Geosciences 144, 104571. https://doi.org/10.1016/j.cageo.2020.104571.

He, C., Li, Q., Liou, K.-N., Takano, Y., Gu, Y., Qi, L., Mao, Y., Leung, L.R., 2014. Black carbon radiative forcing over the Tibetan Plateau. Geophysical Research Letters 41, 7806–7813. https://doi.org/10.1002/2014GL062191.

He, S., Smirnova, T.G., Benjamin, S.G., 2019. A Scale-Aware Parameterization for Estimating Subgrid Variability of Downward Solar Radiation Using High-Resolution Digital Elevation Model Data. Journal of Geophysical Research: Atmospheres 124, 13680–13692. https://doi.org/10.1029/2019JD031563.

Hedrick, A.R., Marks, D., Havens, S., Robertson, M., Johnson, M., Sandusky, M., Marshall, H.P., Kormos, P.R., Bormann, K.J., Painter, T.H., 2018. Direct Insertion of NASA Airborne Snow Observatory-Derived Snow Depth Time Series Into the iSnobal Energy Balance Snow Model. Water Resources Research 54 (10), 8045–8063. https://doi.org/10.1029/2018WR023190.

Hedrick, A.R., Marks, D., Marshall, H.P., McNamara, J., Havens, S., Trujillo, E., Sandusky, M., Robertson, M., Johnson, M., Bormann, K.J., Painter, T.H., 2020. From Drought to Flood: A Water Balance Analysis of the Tuolumne River Basin during Extreme Conditions (2015–2017). Hydrological Processes 11 (34). https://doi.org/10.1002/hyp.13749.

Hinkelman, L.M., Lapo, K.E., Cristea, N.C., Lundquist, J.D., 2015. Using CERES SYN Surface Irradiance Data as Forcing for Snowmelt Simulation in Complex Terrain*. Journal of Hydrometeorology 16, 2133–2152. https://doi.org/10.1175/JHM-D-14-0179.1.

Huang, H., Qian, Y., He, C., Bair, E.H., Rittger, K., 2022. Snow Albedo Feedbacks Enhance Snow Impurity-Induced Radiative Forcing in the Sierra Nevada. Geophysical Research Letters 49, e2022G–L098102. https://doi.org/10.1029/2022GL098102.

Hubbard, S.S., Williams, K.H., Agarwal, D., Banfield, J., Beller, H., Bouskill, N., Brodie, E., Carroll, R., Dafflon, B., Dwivedi, D., Falco, N., Faybishenko, B., Maxwell, R., Nico, P., Steefel, C., Steltzer, H., Tokunaga, T., Tran, P.A., Wainwright, H., Varadharajan, C., 2018. The East River, Colorado, Watershed: A Mountainous Community Testbed for Improving Predictive Understanding of Multiscale Hydrological-Biogeochemical Dynamics. Vadose Zone Journal 17. https://doi.org/10.2136/vzj2018.03.0061.

James, E.P., Alexander, C.R., Dowell, D.C., Weygandt, S.S., Benjamin, S.G., Manikin, G. S., Brown, J.M., Olson, J.B., Hu, M., Smirnova, T.G., Ladwig, T., Kenyon, J.S., Turner, D.D., 2022. The High-Resolution Rapid Refresh (HRRR): An Hourly Updating Convection-Allowing Forecast Model. Part II: Forecast Performance. Weather and Forecasting 37, 1397–1417. https://doi.org/10.1175/WAF-D-21-0130.1.

Kaempfer, T.U., Schneebeli, M., 2007. Observation of isothermal metamorphism of new snow and interpretation as a sintering process. Journal of Geophysical Research: Atmospheres 112. https://doi.org/10.1029/2007JD009047.

Kiewiet, L., Trujillo, E., Hedrick, A.R., Havens, S., Hale, K., Seyfried, M., Kampf, S., Godsey, S.E., 2022. Effects of spatial and temporal variability in surface water inputs on streamflow generation and cessation in the rain–snow transition zone. Hydrology and Earth System Sciences 26 (10), 2779–2796. https://doi.org/10.5194/hess-26-2779-2022.

Kormos, P.R., Marks, D., McNamara, J.P., Marshall, H.P., Winstral, A., Flores, A.N., 2014. Snow distribution, melt and surface water inputs to the soil in the mountain rain–snow transition zone. Journal of Hydrology 519, 190–204. https://doi.org/10.1016/j.jhydrol.2014.06.051.

Krinner, G., Derksen, C., Essery, R., Flanner, M., Hagemann, S., Clark, M., Hall, A., Rott, H., Brutel-Vuilmet, C., Kim, H., Ménard, C.B., Mudryk, L., Thackeray, C., Wang, L., Arduini, G., Balsamo, G., Bartlett, P., Boike, J., Boone, A., Chéruy, F., Colin, J., Cuntz, M., Dai, Y., Decharme, B., Derry, J., Ducharne, A., Dutra, E., Fang, X., Fierz, C., Ghattas, J., Gusev, Y., Haverd, V., Kontu, A., Lafaysse, M., Law, R., Lawrence, D., Li, W., Marke, T., Marks, D., Ménégoz, M., Nasonova, O., Nitta, T., Niwano, M., Pomeroy, J., Raleigh, M.S., Schaedler, G., Semenov, V., Smirnova, T.G., Stacke, T., Strasser, U., Svenson, S., Turkov, D., Wang, T., Wever, N., Yuan, H., Zhou, W., Zhu, D., 2018. ESM-SnowMIP: assessing snow models and quantifying snow-related climate feedbacks. Geoscientific Model Development 11, 5027–5049. https://doi.org/10.5194/gmd-11-5027-2018.

Lapo, K.E., Hinkelman, L.M., Raleigh, M.S., Lundquist, J.D., 2015. Impact of errors in the downwelling irradiances on simulations of snow water equivalent, snow surface temperature, and the snow energy balance. Water Resources Research 51, 1649–1670. https://doi.org/10.1002/2014WR016259.

Lapo, K.E., Hinkelman, L.M., Sumargo, E., Hughes, M., Lundquist, J.D., 2017. A critical evaluation of modeled solar irradiance over California for hydrologic and land surface modeling. JGR Atmospheres 122, 299–317. https://doi.org/10.1002/2016JD025527.

Lee, T.R., Leeper, R.D., Wilson, T., Diamond, H.J., Meyers, T.P., Turner, D.D., 2023. Using the U.S. Climate Reference Network to Identify Biases in Near- and Subsurface Meteorological Fields in the High-Resolution Rapid Refresh (HRRR) Weather Prediction Model. Weather and Forecasting 38, 879–900. https://doi.org/10.1175/WAF-D-22-0213.1.

Liou, K.N., Takano, Y., He, C., Yang, P., Leung, L.R., Gu, Y., Lee, W.L., 2014. Stochastic parameterization for light absorption by internally mixed BC/dust in snow grains for application to climate models. Journal of Geophysical Research: Atmospheres 119, 7616–7632. https://doi.org/10.1002/2014JD021665.

Malik, M.J., van der Velde, R., Vekerdy, Z., Su, Z., 2012. Assimilation of Satellite-Observed Snow Albedo in a Land Surface Model. Journal of Hydrometeorology 13, 1119–1130. https://doi.org/10.1175/JHM-D-11-0125.1.

Marks, D., Domingo, J., Susong, D., Link, T., Garen, D., 1999. A spatially distributed energy balance snowmelt model for application in mountain basins. Hydrological Processes 13, 1935–1959. https://doi.org/10.1002/(SICI)1099-1085(199909)13:12/13<1935::AID-HYP868>3.0.CO;2-C.

Marks, D., Dozier, J., 1992. Climate and energy exchange at the snow surface in the Alpine Region of the Sierra Nevada: 2. Snow cover energy balance. Water Resources Research 28, 3043–3054. https://doi.org/10.1029/92WR01483.

Marks, D., Winstral, A., 2001. Comparison of Snow Deposition, the Snow Cover Energy Balance, and Snowmelt at Two Sites in a Semiarid Mountain Basin. Journal of Hydrometeorology 2 (3), 213–227. https://doi.org/10.1175/1525-7541(2001)002<0213:COSDTS>2.0.CO;2.

Meyer, J., Horel, J., Kormos, P., Hedrick, A., Trujillo, E., Skiles, S.M., 2023. Operational water forecast ability of the HRRR-iSnobal combination: an evaluation to adapt into production environments. Geosci. Model Dev. 16, 233–250. https://doi.org/10.5194/gmd-16-233-2023.

Miller, S.D., Wang, F., Burgess, A.B., Skiles, S.M., Rogers, M., Painter, T.H., 2016. Satellite-Based Estimation of Temporally Resolved Dust Radiative Forcing in Snow Cover. Journal of Hydrometeorology 17, 1999–2011. https://doi.org/10.1175/JHM-D-15-0150.1.

Minder, J.R., Letcher, T.W., Skiles, S.M., 2016. An evaluation of high-resolution regional climate model simulations of snow cover and albedo over the Rocky Mountains, with implications for the simulated snow-albedo feedback. Journal of Geophysical Research: Atmospheres 121, 9069–9088. https://doi.org/10.1002/2016JD024995.

Niwano, M., Aoki, T., Kuchiki, K., Hosaka, M., Kodama, Y., Yamaguchi, S., Motoyoshi, H., Iwata, Y., 2014. Evaluation of updated physical snowpack model SMAP. Bulletin of Glaciological Research 32, 65–78. https://doi.org/10.5331/bgr.32.65.

Niwano, M., Kajino, M., Kajikawa, T., Aoki, T., Kodama, Y., Tanikawa, T., Matoba, S., 2021. Quantifying Relative Contributions of Light-Absorbing Particles From Domestic and Foreign Sources on Snow Melt at Sapporo, Japan During the 2011–2012 Winter. Geophysical Research Letters 48, e2021G–L093940. https://doi.org/10.1029/2021GL093940.

Oaida, C.M., Xue, Y., Flanner, M.G., Skiles, S.M., De Sales, F., Painter, T.H., 2015. Improving snow albedo processes in WRF/SSiB regional climate model to assess impact of dust and black carbon in snow on surface energy balance and hydrology over western U.S.: Physical snow processes with WRF/SSiB. J. Geophys. Res. Atmos. 120, 3228–3248. https://doi.org/10.1002/2014JD022444.

Painter, T.H., Rittger, K., McKenzie, C., Slaughter, P., Davis, R.E., Dozier, J., 2009. Retrieval of subpixel snow covered area, grain size, and albedo from MODIS. Remote Sensing of Environment 113, 868–879. https://doi.org/10.1016/j.rse.2009.01.001.

Painter, T.H., Bryant, A.C., Skiles, S.M., 2012. Radiative forcing by light absorbing impurities in snow from MODIS surface reflectance data. Geophysical Research Letters 39. https://doi.org/10.1029/2012GL052457.

Pedersen, C.A., Winther, J.-G., 2005. Intercomparison and validation of snow albedo parameterization schemes in climate models. Climate Dynamics 25, 351–362. https://doi.org/10.1007/s00382-005-0037-0.

Qu, X., Hall, A., 2014. On the persistent spread in snow-albedo feedback. Clim Dyn 42, 69–81. https://doi.org/10.1007/s00382-013-1774-0.

Quéno, L., Karbou, F., Vionnet, V., Dombrowski-Etchevers, I., 2020. Satellite-derived products of solar and longwave irradiances used for snowpack modelling in mountainous terrain. Hydrol. Earth Syst. Sci. 24, 2083–2104. https://doi.org/10.5194/hess-24-2083-2020.

Rast, M., Nieke, J., Adams, J., Isola, C., Gascon, F., 2021. Copernicus Hyperspectral Imaging Mission for the Environment (Chime), in: 2021 IEEE International Geoscience and Remote Sensing Symposium IGARSS. Presented at the 2021 IEEE International Geoscience and Remote Sensing Symposium IGARSS, pp. 108–111. Doi: 10.1109/IGARSS47720.2021.9553319.

Rittger, K., Bormann, K.J., Bair, E.H., Dozier, J., Painter, T.H., 2021. Evaluation of VIIRS and MODIS Snow Cover Fraction in High-Mountain Asia Using Landsat 8 OLI. Frontiers in Remote Sensing 2.

Rittger, K., Raleigh, M.S., Dozier, J., Hill, A.F., Lutz, J.A., Painter, T.H., 2020. Canopy Adjustment and Improved Cloud Detection for Remotely Sensed Snow Cover Mapping. Water Resources Research 56. https://doi.org/10.1029/2019WR024914.

Ryken, A., Bearup, L.A., Jefferson, J.L., Constantine, P., Maxwell, R.M., 2020. Sensitivity and model reduction of simulated snow processes: Contrasting observational and parameter uncertainty to improve prediction. Advances in Water Resources 135, 103473. https://doi.org/10.1016/j.advwatres.2019.103473.

Sarangi, C., Qian, Y., Rittger, K., Bormann, K.J., Liu, Y., Wang, H., Wan, H., Lin, G., Painter, T.H., 2019. Impact of light-absorbing particles on snow albedo darkening and associated radiative forcing over high-mountain Asia: high-resolution WRF-Chem modeling and new satellite observations. Atmospheric Chemistry and Physics 19, 7105–7128. https://doi.org/10.5194/acp-19-7105-2019.

Schmucki, E., Marty, C., Fierz, C., Lehning, M., 2014. Evaluation of modelled snow depth and snow water equivalent at three contrasting sites in Switzerland using SNOWPACK simulations driven by different meteorological data input. Cold Regions Science and Technology 99, 27–37. https://doi.org/10.1016/j.coldregions.2013.12.004.

Skiles, S.M., Donahue, C.P., Hunsaker, A.G., Jacobs, J.M., 2023. UAV hyperspectral imaging for multiscale assessment of Landsat 9 snow grain size and albedo. Frontiers in Remote Sensing 3.

Skiles, S.M., Painter, T.H., Deems, J.S., Bryant, A.C., Landry, C.C., 2012. Dust radiative forcing in snow of the Upper Colorado River Basin: 2. Interannual variability in radiative forcing and snowmelt rates: DUST RADIATIVE FORCING SNOWMELT RESPONSE. Water Resour. Res. 48. Doi: 10.1029/2012WR011986.

Skiles, S.M., Painter, T., 2017. Daily evolution in dust and black carbon content, snow grain size, and snow albedo during snowmelt, Rocky Mountains, Colorado. Journal of Glaciology 63, 118–132. https://doi.org/10.1017/jog.2016.125.

Skiles, S.M., Painter, T.H., 2019. Toward Understanding Direct Absorption and Grain Size Feedbacks by Dust Radiative Forcing in Snow With Coupled Snow Physical and Radiative Transfer Modeling. Water Resour. Res. 55, 7362–7378. https://doi.org/10.1029/2018WR024573.

Smirnova, T.G., Brown, J.M., Benjamin, S.G., Kenyon, J.S., 2016. Modifications to the Rapid Update Cycle Land Surface Model (RUC LSM) Available in the Weather Research and Forecasting (WRF) Model. Mon. Wea. Rev. 144, 1851–1865. https://doi.org/10.1175/MWR-D-15-0198.1.

Steger, C.R., Steger, B., Schär, C., 2022. HORAYZON v1.2: an efficient and flexible ray-tracing algorithm to compute horizon and sky view factor. Geoscientific Model Development 15, 6817–6840. https://doi.org/10.5194/gmd-15-6817-2022.

Stillinger, T., Rittger, K., Raleigh, M.S., Michell, A., Davis, R.E., Bair, E.H., 2023. Landsat, MODIS, and VIIRS snow cover mapping algorithm performance as validated by airborne lidar datasets. The Cryosphere 17, 567–590. https://doi.org/10.5194/tc-17-567-2023.

Tuzet, F., Dumont, M., Lafaysse, M., Picard, G., Arnaud, L., Voisin, D., Lejeune, Y., Charrois, L., Nabat, P., Morin, S., 2017. A multilayer physically based snowpack model simulating direct and indirect radiative impacts of light-absorbing impurities in snow. The Cryosphere 11, 2633–2653. https://doi.org/10.5194/tc-11-2633-2017.

Winstral, A.H., Marks, D., Gurney, R., 2009. An efficient method for distributing wind speeds over heterogeneous terrain. Hydrological Processes 23 (17), 2526–2535. https://doi.org/10.1002/hyp.7141.

Wiscombe, W.J., Warren, S.G., 1980. A Model for the Spectral Albedo of Snow. I: Pure Snow. Journal of the Atmospheric Sciences 37, 2712–2733. https://doi.org/10.1175/1520-0469(1980)037<2712:AMFTSA>2.0.CO;2.